Received: 16 September 2020 | Revised: 14 June 2021 | Accepted: 15 June 2021 | Published on: 29 June 2021

DOI: 10.1002/joc.7262

RESEARCH ARTICLE

International Journal of Climatology RMetS

Extreme winds and fire weather in coastal Santa Barbara County, CA: An observational analysis

Katelyn Zigner[1] | **Leila M. V. Carvalho**[1,2] | **Charles Jones**[1,2] | **Gert-Jan Duine**[2]

[1]Department of Geography, University of California, Santa Barbara, California, USA

[2]Earth Research Institute, University of California, Santa Barbara, California, USA

Correspondence
Katelyn Zigner, Department of Geography, University of California, Santa Barbara, California, 93106, USA.
Email: kzigner@ucsb.edu

Funding information
National Science Foundation, Grant/Award Number: PREEVENTS ICER - 1664173

Abstract

Coastal Santa Barbara (SB) County in Southern California, characterized by a Mediterranean climate and complex topography, is a region prone to downslope windstorms that create critical fire weather conditions and rapidly spread wildfires. The Santa Ynez Mountains, oriented from east to west, rise abruptly from the coast, separating air masses from the ocean and the Santa Ynez Valley. The juxtaposition of these geographic features generates spatiotemporally variable wind regimes. This study analyzes diurnal-to-seasonal wind cycles and extremes in this region using hourly data from eight weather stations and four buoys for the period 1998–2019. Data from a vertical wind profiler at the Santa Barbara airport in Goleta, CA was extracted from August 2016 to September 2020. Air temperature, dew point temperature, and the Fosberg fire weather index are examined at land stations. We show that cycles in wind speed vary spatiotemporally; mountain (valley and coastal) stations exhibit a pronounced semiannual (annual) cycle, and wind maxima is observed during the evening (afternoon) at mountain (valley and coastal) stations. Differences in wind speed percentiles were evident among stations, particularly at and above the 75th percentile. Strong winds recorded at buoys were significantly correlated (between $r = 0.3$–0.5) to land stations. However, cross-correlational analysis did not reveal any temporal lags between mountain stations and buoys. Distributions of temperature and dew point during extreme winds differed between east and west mountain stations. Significant fire weather conditions were most frequent at mountain stations in Refugio and Montecito, with 5% occurrence in the spring and over 3% occurrence in fall. Weaker summertime winds lowered fire weather conditions at Montecito in the summer.

KEYWORDS

extreme winds, fire weather, Mediterranean climate, mountain winds, Southern California, Sundowner winds, thermally driven circulations

1 | INTRODUCTION

Coastal Southern California is characterized by a Mediterranean climate, with dry summers and wet winters. Nonetheless, regional differences in climate are attributed to the complex terrain spanning the U.S. West Coast. Santa Barbara (SB) County, situated in Southern California, provides an example of a region where

topography and proximity to the ocean creates spatiotemporal variability in atmospheric variables. With a 100 km length, 10 km width, and peaks over 1.2 km above sea level, the Santa Ynez Mountains (SYM) exhibit a distinctive east–west orientation and separate the cool Pacific Ocean from the Santa Ynez Valley (SYV). The San Rafael Mountains, north of the SYM with peak elevations exceeding 2 km, help create the "v-shape" of the SYV (Figure 1). The complex terrain and oceanic influence generate interacting thermally driven wind circulations along the coast (Dorman and Winant, 2000), on the slopes of the SYM, and along the SYV to the north (Jones et al., 2021).

Another unique feature of the region is the downslope windstorm frequently observed on the southern SYM slopes. These cross-mountain (northerly) winds are known as "Sundowners" due to their typical onset near sunset (Ryan, 1991; Ryan, 1996; Blier, 1998; Cannon et al., 2017; Smith et al., 2018a, 2018b; Duine et al., 2019, 2021; Carvalho et al., 2020; Jones et al., 2021). Sundowners are infamous for their role in rapidly spreading wildfires that often disrupt the community of ~130,000 inhabitants living in coastal SB (Zigner et al., 2020). The National Weather Service Oxnard/Los Angeles (henceforth NWS-LOX) is particularly concerned about these cross-mountain (northerly) winds when sustained speeds reach 13.4 m/s (30 mph) or gusts reach 15.6 m/s (35 mph; NWS-LOX, personal communication). Sundowners may produce gale-force winds and critically low relative humidity (<15%; Sukup, 2013; Cannon et al., 2017; Carvalho et al., 2020; Jones et al., 2021). Although temperature ramps do not occur during all Sundowners (Blier, 1998; Carvalho et al., 2020), a handful of past events have reported atypically hot temperatures after sunset, exceeding 30°C during some summer Sundowners (Ryan, 1991; Ryan, 1996; Blier, 1998; Zigner et al., 2020).

Wildfire behaviour is driven by fuels, topography, and weather (Countryman, 1972). However, weather is the leading factor in wildfire spread and intensity during extreme winds (Rothermel, 1983; Keeley et al., 2009; Moritz et al., 2010). Locally, the NWS-LOX defines "Red Flag Criteria" in most of southern California as dry fuels with any one of: (a) relative humidity (RH) ≤ 15% with sustained winds ≥25 mph or gusts ≥35 mph for 6 hr, (b) RH ≤ 10% with sustained winds ≥15 mph or gusts

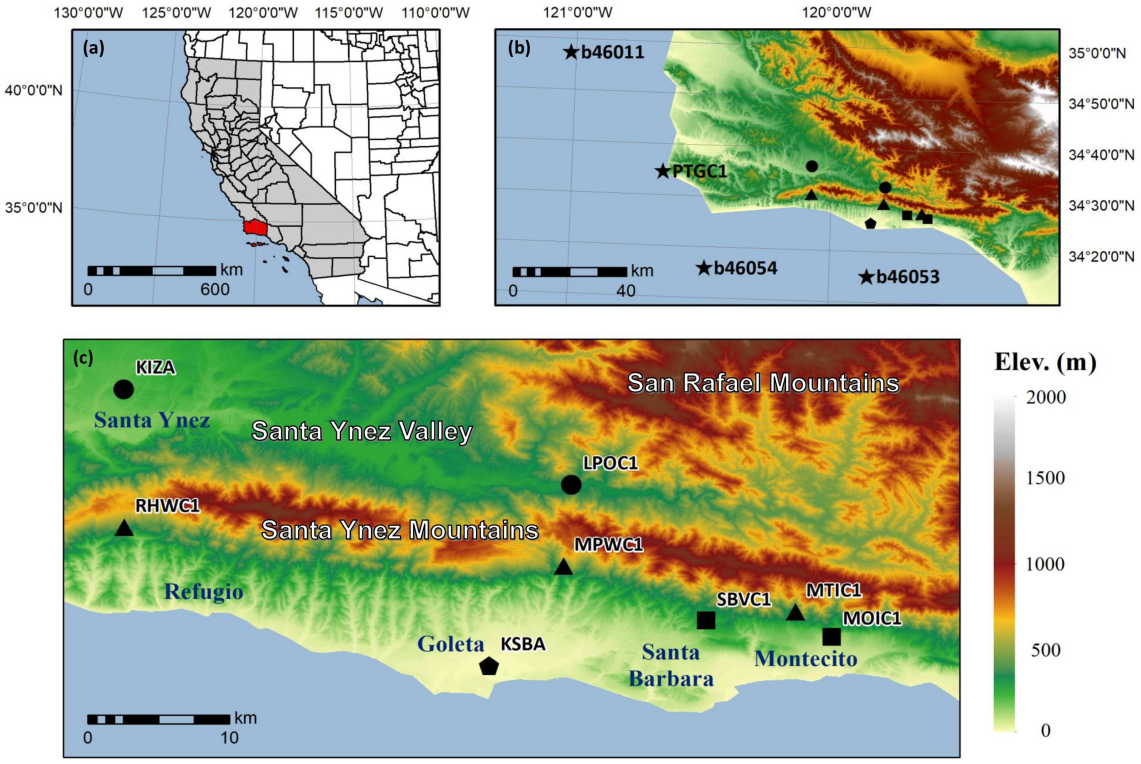

FIGURE 1 (a) California counties (shaded) and Santa Barbara County. (b) Digital elevation model of Santa Barbara County with land stations and buoys. Shapes identify station categorization used throughout the article: Valley (circle), mountain (triangle), foothill (square), coast (pentagon), and buoy (star). Station details are provided in Table 1. (c) Further detail of land stations, showing multiple ridges and valleys on the south side of the Santa Ynez Mountains. Cities are also identified [Colour figure can be viewed at wileyonlinelibrary.com]

≥25 mph for 6 hr, (c) widespread and/or significant dry lightning, or (d) forecaster discretion (typically used with RH close to the criteria in (a) or (b) and very strong winds; National Weather Service Lox Angeles/Oxnard, 2021). Thus, Sundowners may create significant fire weather conditions. With expansion into the wildland-urban interface served by a few narrow and winding roads (see Figure S1 for imagery of this area), understanding the spatiotemporal variability of strong winds and fire weather is critical to identify particularly at-risk regions and thus improve fire resource planning and focus preventative measures, ultimately increasing community resilience to wildfires.

The bulk of knowledge regarding winds in SB is based on regional models focusing on Sundowner winds (Cannon et al., 2017; Hatchett et al., 2018; Smith et al., 2018a, 2018b; Duine et al., 2019, 2021; Carvalho et al., 2020; Jones et al., 2021). These studies showed spatial and temporal variability in wind speed and direction on the SYM slopes during these events. The Sundowner Winds Pilot Experiment (Carvalho et al., 2020) examined radiosonde and station data from a Sundowner event in April 2019 and found spatial differences in wind speed and direction along the SYM. Radiosonde profiles of winds and potential temperature (stability) indicated that Sundowners are associated with a lee slope jet and mountain waves, in agreement with model output examining Sundowners in Smith et al. (2018a), Duine et al. (2019), and Jones et al. (2021). Using 30 years of hourly mesoscale simulations, Jones et al. (2021) identified three distinct Sundowner wind regimes (East, West, and Santa Barbara). Spatial and temporal characteristics differentiate the regimes, including the magnitude of winds on the southern SYM slopes and the strength and position of the coastal jet, which forms from synoptic pressure gradients and depth and dynamics of the marine boundary layer (Skyllingstad et al., 2001; Koracin et al., 2004; Dorman and Koračin, 2008; Parish et al., 2014).

No previous study to date has investigated diurnal and seasonal cycles of winds based on observations, including the relationships between winds in the SYV, on the SYM, and in coastal SB using station data. Dorman and Winant (2000) studied winds in the Santa Barbara Channel using primarily buoy data, but that study did not extensively analyse land-based weather stations nor examine relationships between winds in the Santa Barbara channel and Sundowners. Furthermore, although destructive wildfires have undoubtedly impacted SB (Zigner et al., 2020) and previous studies have examined the spatiotemporal variability of Sundowner events, no study has analysed the spatial or temporal variability in extreme fire weather conditions in this region.

The primary objective of this study is to develop an in-depth analysis of surface winds and fire weather in coastal SB utilizing long-term observational station data and the National Oceanic and Atmospheric Administration (NOAA) wind profiler installed at the Santa Barbara airport. The main scientific questions investigated in this manuscript are as follows: (a) Are east and west Sundowner regimes distinct and evident from data collected at weather stations? (b) Are strong surface winds at buoys near Point Conception (to the west of SB) and in the Santa Barbara channel related to strong winds at land-based stations? and (c) Do extreme fire weather conditions vary among mountain locations? These issues will be examined by calculating various wind statistics, including diurnal-to-seasonal cycles, percentiles, and correlations. Additional meteorological variables such as temperature and dew point are analysed during extreme winds, and a fire weather index is used to determine the frequency of significant fire weather conditions. Advancing knowledge of spatial and temporal wind and fire weather patterns in coastal SB using observations have practical applications in weather forecasting and climate investigations. Moreover, the statistical analyses provided here based on stations may enable improvements in resource allocation, including the placement of new stations and profilers, potentially contributing to strategic fuel management, minimizing risk around homes and other structures (McWethy et al., 2019; Miller et al., 2020). These results can be useful for the creation of in situ fire management strategies, as proposed in Thompson et al. (2016), and contribute to evacuation planning in a region highly vulnerable to wildfires (Li et al., 2019). Finally, the proposed methods can potentially contribute to understanding wind regimes in other coastal regions dominated by Mediterranean climate and exhibiting complex topography.

The article is organized as follows. Section 2 explains the data and processing methods. Section 3 explores diurnal-to-seasonal wind cycles, wind percentiles, the application of the NWS-LOX Sundowner criteria at each station, correlations between land and buoy stations, and utilization of data from the wind profiler. Section 4 analyzes diurnal and seasonal cycles of temperature, relative humidity, dew point, and examines variability during extreme winds. Section 5 examines variability in fire weather through the use of a fire weather index, and Section 6 provides a discussion and summary of the main findings.

2 | DATA AND METHODS

Data were obtained from eight land-based stations through the MesoWest network (Horel et al., 2002) in coastal SB and the SYV (Table 1). Stations were

TABLE 1 Information on weather stations including location, elevation, operating agency (NWS: National Weather Service, USFS: US Forest Service, NDBC: National Data Buoy Centre), and temporal data collection details

Station ID	Station name	Latitude	Longitude	Elevation (m)	Agency	Reporting time (min s^{-1})	Station installation
KIZA	Santa Ynez Airport	34.607	−120.076	205	NWS	Varied over time	April 2005
KSBA	Santa Barbara airport	34.426	−119.844	3	NWS	Varied over time	November 1998
LPOC1	Los Prietos	34.544	−119.791	299	USFS	10, 14, 35	December 1999
MOIC1	Montecito #2	34.445	−119.626	87	USFS	07	April 2011
MPWC1	San Marcos pass	34.491	−119.796	454	USFS	06	July 2015
MTIC1	Montecito	34.461	−119.649	493	USFS	10, 14, 47	January 2000
RHWC1	Refugio	34.517	−120.075	447	USFS	06	July 2015
SBVC1	Santa Barbara botanic garden	34.456	−119.706	230	USFS	24	June 2011
b46011	Santa Maria	34.956	−121.019	0	NDBC	00, 10, 20, 30, 40, 50	January 1998
B46053	East Santa Barbara	34.252	−119.853	0	NDBC	00, 10, 20, 30, 40, 50	January 1998
b46054	West Santa Barbara	34.265	−120.477	0	NDBC	00, 10, 20, 30, 40, 50	January 1998
PTGC1	Point Arguello	34.577	−120.648	0	NDBC	00, 10, 20, 30, 40, 50	January 1998

Note: Stations LPOC1 and MTIC1 changed reporting times in their history, hence the multiple reporting times. All NDBC-owned stations recorded hourly data until the mid-2010's when all began collecting data every 10 min.

categorized into four classes based on location and elevation: valley, mountain, foothill, and coastal (Figures 1 and S1). Mountain stations are located on the southern SYM slopes above foothill stations. Few stations were available closer to the SYM crest (within 250 m), and these stations were not selected for analysis because of the short time periods for data collection at the time of manuscript submission (<3 years of data). Furthermore, the majority of these stations have not followed standard protocols for sensor installation, as implemented by the NWS and U.S. Forest Service, unlike the other stations selected in this study. Therefore, all stations analysed in this study maintain the standards set among government-owned stations. The single coastal station (KSBA) has the lowest elevation and is situated <1.5 km from the coast. This station was separated from other groups because of the potential influence of the marine boundary layer, shown more subtly at all other stations. Additional data were collected from three National Data Buoy Centre (NDBC) buoys in the Santa Barbara Channel and near Point Conception to the west (see Figure 1b for location); a land station available from the NDBC was added since it represents a key location in the western part of the analysis domain.

Data was downloaded from the installation date to August 2019. The variable installation dates (see Table 1) affected the number of observations available at stations. Initial quality control was undergone by the MesoWest data network and the NDBC. Additional quality control data analysis was performed by evaluating the existence of discontinuities or abrupt shifts in means, upper and lower percentiles, caused by changes in instrument sensor. We extracted and examined sample outliers in wind speed, temperature, and dew point, and found no evidence of erroneous data. Hence, all data provided by the data networks were utilized.

The land-based stations are comprised of both NWS Automated Service Observation Stations (ASOS) and U.S. Forest Service Remote Automated Weather Stations (RAWS; National Wildfire Coordinating Group). Inherent differences exist between ASOS and RAWS. Wind instruments on ASOS are installed 10 m above ground level and calculate sustained wind speed as the average wind over a 2 min period from a 5 sec sampling frequency. RAWS wind instruments are installed 6.1 m above ground level and calculate sustained wind speed as the average wind over a 10 min period from a 3 s sampling frequency. Temperature and humidity sensors are placed at 2 m above ground level for ASOS and 1.2–2.4 m above ground level for RAWS following the protocols of the National Wildfire Coordinating Group (2014).

Reporting times for observations vary between the agencies; ASOS report subhourly data, RAWS report hourly data, and NDBC report hourly and subhourly data depending on the buoy or station. To compare among stations, data were processed to create one representative data point per hour. This was completed using different techniques depending on the number of observations per hour and the time of the observations. At stations with one reported observation per hour recorded between

15 min prior to and 15 min after the hour (LPOC1, MOIC1, MPWC1, MTIC1, and RHWC1), the recorded observation was used. For example, the processed data at 0600 PST at RHWC1 was the observation recorded at 0606 PST. At stations with one observation per hour recorded between 15 min and 45 min after the hour (LPOC1 and SBVC1), the observations in the aforementioned 30 min period before and after each hour were averaged. For example, the processed data point 0600 PST at SBVC1 was calculated by averaging the observations at 0524 and 0624 PST. At stations with subhourly observations (KIZA, KSBA, and all NDBC stations), we averaged all observations between 15 min prior and 15 min after the hour. For example, the processed data point 0600 PST at KSBA was calculated by averaging all observations between 0545 and 0615 PST.

In addition to data from land stations, hourly vertical wind data were obtained from a NOAA Physical Sciences Laboratory 449 MHz wind profiler (Ecklund et al., 1988) located at the Santa Barbara airport from August 2016 to September 2020. Wind profilers transmit electromagnetic pulses vertically in at least two slightly different directions (~75°), which allow for analysis of winds in three dimensions. A signal-to-noise ratio is used to determine atmospheric phenomena (i.e., clouds, precipitation) from nonmeteorological obstructions (i.e., birds, planes). In particular, the type of wind profiler at the Santa Barbara airport uses a coaxial-colinear phased array antenna with a peak transmit power of 2000 W. Hourly data was obtained, typically ranging from 200 m to 8 km above ground level (AGL) with a vertical resolution of approximately 100 m. This data provided a complementary analysis into the vertical wind profile of seasonal and diurnal cycles, and during Sundowner events.

Fire weather indices can identify critical fire weather conditions that may facilitate rapid wildfire spread. One widely used fire weather index is the Fosberg Fire Weather Index (FFWI; Fosberg, 1978). The FFWI calculates the small-scale and short-term (e.g., hourly) fire weather conditions using wind speed, temperature, and relative humidity (Goodrick, 2002). The FFWI and the National Fire Danger Rating System are used operationally to forecast areas of enhanced fire threat. Studies such as Jones et al. (2010) and Moritz et al. (2010) have used the FFWI to examine fire weather conditions during Santa Ana wind events. We used the FFWI to examine areas at high risk of wildfire spread due to extreme winds in coastal SB.

The FFWI is defined as:

$$\mathrm{FFWI}=\frac{\eta * \sqrt{1+U^2}}{0.3002}$$

where U is wind speed in mph, and η is the moisture damping coefficient, defined as:

$$\eta=1-2\left(\frac{m}{30}\right)+1.5\left(\frac{m}{30}\right)^2-0.5\left(\frac{m}{30}\right)^3$$

The equilibrium moisture content (m) is a function of temperature in degrees Fahrenheit (t) and relative humidity in percent (h), given by:

$$m=\begin{cases}\text{for } h\leq 10\%: \\ 0.03229+0.281073h-0.000578ht \\ \text{for } 10\%<h\leq 50\%: \\ 2.22749+0.160107h-0.01478t \\ \text{for } h>50\%: \\ 21.0606+0.005565h^2-0.00035ht-0.483199h\end{cases}$$

To account for precipitation, $m = 30$ when precipitation reaches 0.25 mm in the previous 24 hr, as applied to Santa Ana Winds in Jones et al. (2010). The FFWI ranges between 0 and 100, reaching 100 when RH is 0% and wind speed is 30 mph. FFWI values exceeding 50 are considered significant for fire weather on a national scale (Goodrick, 2002; Hazra et al., 2018).

Seasonal (diurnal) cycles of wind speed, temperature, dew point, and FFWI were created by calculating the daily (hourly) mean and fitting the first two harmonics. For the correlations among and between land and buoy stations, significance was assessed by applying a nonparametric test based on Monte Carlo resampling. The test was constructed by randomly resampling the time series for each pair of stations 10,000 times (using the number of matching data points) and calculating the linear Pearson's correlation coefficient between the pair. The Ho hypothesis (no correlation) was rejected if the absolute value of the correlation was greater than the 95th or 99th percentile of the absolute value of the respective random distribution. When we compared Sundowner versus non-Sundowner days using the vertical wind profiler, statistical significance was determined using a Student's t-statistic for and u and v wind components. In this case, we reject Ho if either u or v are statistically significant at the 5% significance level.

To analyse variations in temperature and dew point during Sundowners (as defined by the NWS-LOX wind criteria), we calculated hourly medians of temperature and dew point during hours not reaching Sundowner criteria for each season and compared with temperature and dew point data during Sundowners. The number of hours that reached Sundowner criteria in each season ranged between 0 to 216 hr at MTIC1 and 3 to 134 hr at RHWC1 (length of records is different for each station;

see Table 1). Thus, given the large difference in sample sizes between non-Sundowner and Sundowner hours and the unknown distributions of these differences, we assessed the statistical significance in the differences in medians based on a nonparametric test. For this test, we constructed a distribution of 10,000 random samples extracted from non-Sundowner data separated by hour and season. Each one of these sampled of non-Sundowner hours have the same number of records as the Sundowner hours. Then, the median of the Sundowner data for the matching season/hour was compared to the resulting distribution of the non-Sundowner medians. The null hypothesis is that the Sundowner medians do not differ from randomly obtained medians of the non-Sundowner cases. We reject the null hypothesis at the 9fifth confidence interval if the Sundowner median was less than the 2.fifth percentile or greater than the 97.5th percentile (considering a two-tail test) of the respective distribution of non-Sundowner medians. For example, there are 195 hr that reached the NWS Sundowner criteria at MTIC1 in spring (March–May) at 00z. For this season and hour, 195 non-Sundowner hours were randomly sampled with replacement 10,000 times to create a distribution. The median of the Sundowner occurrences was then compared to the percentiles of the non-Sundowner distribution, and this process was completed for all seasons and hours individually.

3 | OBSERVED WIND PATTERNS AND EXTREMES

3.1 | Seasonal

We start by first presenting the seasonal variability of mean winds at ASOS and RAWS. Valley, foothill, and coastal (henceforth "nonmountain") stations exhibit a distinct wind pattern compared to mountain stations, with nonmountain stations reporting a smaller seasonal wind speed range (<1 m/s) and no bimodal pattern in mean wind speed (Figure 2). Mountain stations record the highest wind speeds, largest range in wind speeds, and exhibit a bimodal pattern throughout the year; wind speeds are strongest in spring, then decrease in summer, and increase again in fall. Additionally, RHWC1 in the west SYM typically records the strongest winds, followed by MPWC1 in the central SYM, and finally MTIC1 in the east SYM. Located on the western SYM (Figure S1b), RHWC1 seems to be strongly influenced by the dominant coastal NW flow and coastal jet (Rahn et al., 2014; Smith et al., 2018b). MPWC1 (central SYM) is near San Marcos Pass, a prominent gap in the central SYM oriented northwest-to-southeast that may contribute to

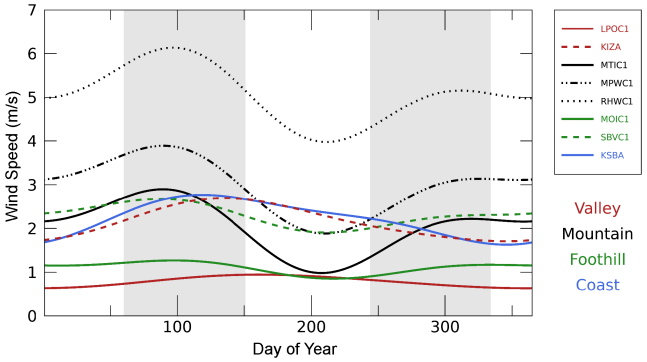

FIGURE 2 Seasonal cycles of wind speed by station. Grey shading in the background indicates spring and fall [Colour figure can be viewed at wileyonlinelibrary.com]

channelling northwesterly winds. MTIC1 (east SYM) is located on a prominent peak on a ridge in the eastern SYM above Montecito with the surrounding canyons oriented northeast-to-southwest (see Figure S1c).

Most stations record maximum wind speeds in spring (March to May), consistent with the highest frequency of Sundowner winds (e.g., Hatchett et al., 2018; Smith et al., 2018a; Jones et al., 2021). Mean wind speeds range between 2–6 m/s at mountain stations and 0.5–3 m/s at nonmountain stations. In summer (Jun - Aug), wind speed decreases at all stations except LPOC1, ranging between 1–5 m/s at mountain stations and 1–3 m/s at nonmountain stations. It should be noted that in summer and early fall, the mean wind speed is commonly larger at KSBA (coast), KIZA (valley), and SBVC1 (east SYM) than at mountain stations MPWC1 (central SYM) and MTIC1 (west SYM). In fall (September to November), wind speed decreases at valley stations and the coastal station, and increases at foothill and mountain stations. Mean wind speed at all stations remains fairly constant until the end of winter when it increases into spring.

3.2 | Diurnal

Similar to the seasonal cycle, the diurnal cycle differs between mountain and nonmountain stations (Figure 3). At mountain stations, the strongest winds occur during the night (between 2000 and 2200 PST). RHWC1, located in the western SYM, records the highest mean magnitude (>6 m/s) and greatest amplitude of the diurnal cycle compared to other stations. Notably, the mean wind speed and amplitudes of the diurnal cycle progressively decrease eastward at mountain stations. Foothill, valley, and coastal stations exhibit a very different diurnal cycle, with the strongest winds observed in the afternoon (between 1200 and 1600 PST) created by to horizontal

pressure gradients creating valley and land-sea circulations. During the day, winds are driven up valley as the inner parts of the valley heat more than the plain (Giovannini et al., 2017). Similarly, the formation of a sea breeze occurs as the land heats more than the ocean, driving onshore daytime winds (Markowski and Richardson, 2010). In the SYV, the sea breeze may reach KIZA and interact with the up-valley circulation (Bastin et al., 2005). Westerly winds are recorded most frequently at valley stations in the summer and least frequently in the winter (not shown). KSBA (coastal) and KIZA (valley) record mean wind speeds in the afternoon that are greater than stations on the slopes of the SYM (Figure 3).

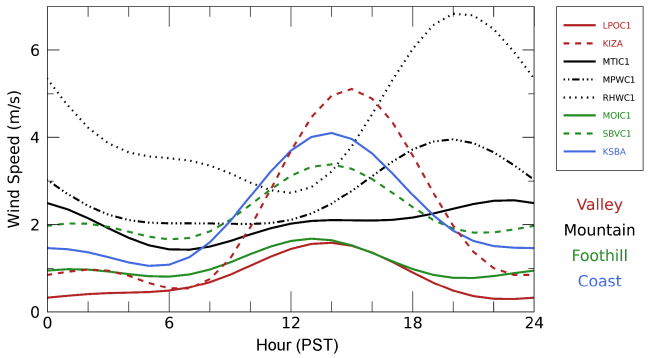

FIGURE 3 Diurnal cycles of wind speed at each station. All months were considered [Colour figure can be viewed at wileyonlinelibrary.com]

The combined frequency of wind speed and direction at each station separated according to the time of the day are assessed based on wind roses (Figures 4 and 5). Only winds at or exceeding 0.5 m/s are shown, since weak winds (<0.5 m/s) are ill-defined for analysis of wind direction. Additionally, the quality control analysis indicated that changes in sensors at some stations have affected the frequency of very light winds (<0.5 m/s). Differences in dominant frequency of wind direction are observed among stations, illustrating the complexity of wind systems in the region. Between 1500 and 1700 PST, most mountain and foothill stations record weak-to-moderate upslope (southerly) winds. The daytime upslope, thermally driven winds are more frequently observed with southeast direction at western station RHWC1, while other mountain stations record weak (<4 m/s), southwesterly winds (Figure 4). These predominant wind orientations could result from the placement of the station in relation to local topographic features (see Figure S1). Approximately 25% of the winds in this time period recorded at RHWC1 are comparatively

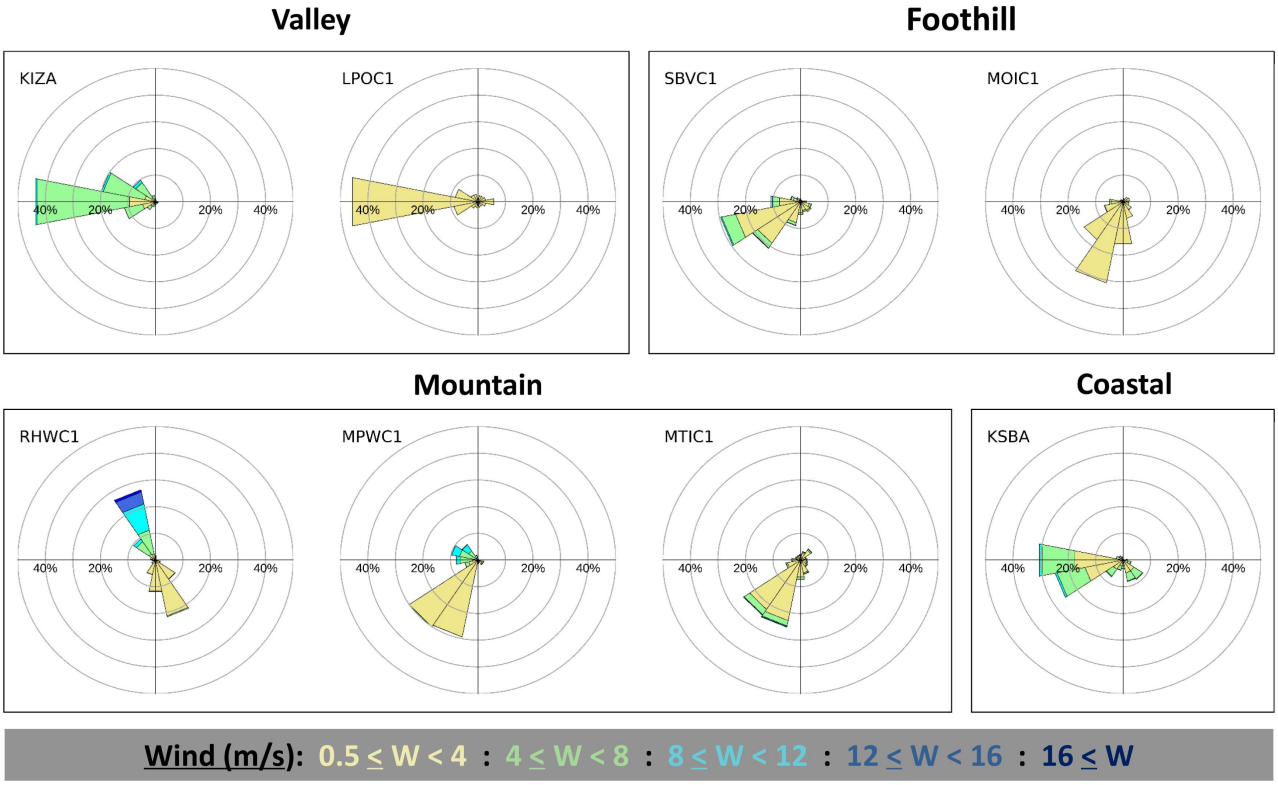

FIGURE 4 Wind roses created using data between 1500 and 1700 PST. Spokes are broken into 22.5° increments, where the length of the spoke indicates wind direction frequency and the colouring indicates wind speed at each direction. Only winds ≥0.5 m/s wind speed threshold were included [Colour figure can be viewed at wileyonlinelibrary.com]

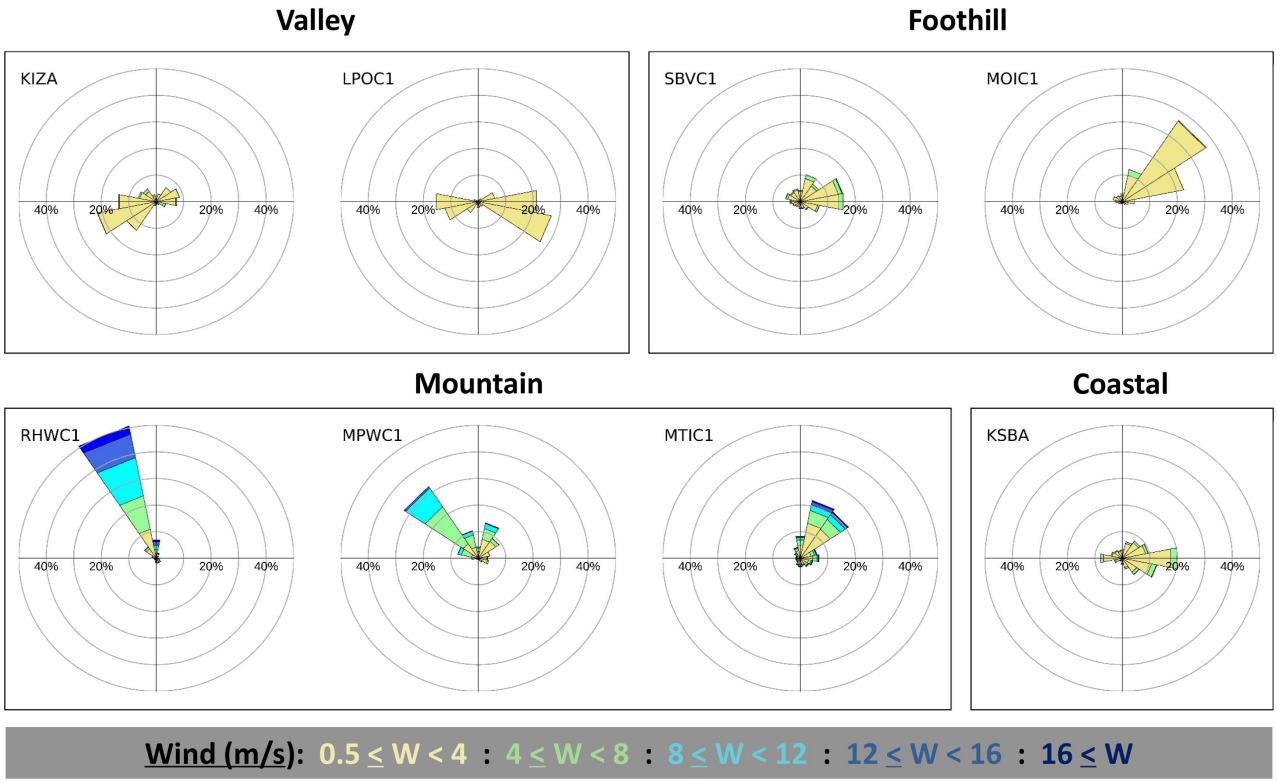

FIGURE 5 Similar to Figure 4 created using data between 2100 and 2300 PST [Colour figure can be viewed at wileyonlinelibrary.com]

northwesterly and strong, commonly exceeding 8 m/s. This can be explained by the persistent northwesterly flow in this region (Dorman and Winant, 2000). Additionally, the strong winds (>8 m/s) recorded between 1500 and 1700 PST at RHWC1 (Figure 4) may reflect contributions from the early onset of Sundowners on the western SYM slopes (Carvalho et al., 2020; Duine et al., 2021; Jones et al., 2021).

We notice a transition from upslope (southerly) to downslope (northerly) winds at most stations on the southern-facing slopes of the SYM in the late afternoon and early evening, as indicated by wind roses from 1800 to 2000 PST (Figure S2) and from 2100 to 2300 PST (Figure 5). Generally, the strongest winds are at mountain stations around 2000 PST (Figure 3) and have northerly components (Figures 4 and 5), continuing through the evening. Radiative surface cooling on the mountain slopes creates downslope (northerly) flow (Markowski and Richardson, 2010; Skyllingstad et al., 2001). The timing and strength of these circulations depend on many factors including slope angle (Nadeau et al., 2013), mountain range orientation with respect to azimuth angle of the sunset, and valley geometric scales (Duine et al., 2017).

Downslope (northerly) wind direction systematically varies along the slopes of the SYM in the evening; downslope winds at RHWC1 (west SYM) and MPWC1 (central SYM) are dominantly northwesterly, whereas eastern SYM stations in the foothills (MOIC1, SBVC1) and on the slopes (MTIC1) exhibit mostly northeasterly winds (Figure 5). The variation in wind directions observed in the west and east regions of the south-facing SYM have been shown in climatological simulations with WRF (Jones et al., 2021). Although more studies are necessary to evaluate all mechanisms explaining the behaviour of wind direction along the slopes of the SYM, sensitivity tests and simulations have shown that the upstream (north) San Rafael Mountains play a critical role in the timing of the onset of the northeasterly winds, and this effect is particularly important in the eastern SYM (Duine et al., 2021).

The coastal station KSBA records a diurnal wind regime consistent with findings regarding flow in the Santa Barbara channel (Dorman and Winant, 2000). This station typically records southeasterly winds around 0900 PST and westerly winds around 1200 PST (not shown) and 1500–1700 PST (Figure 4), transitioning to easterly (onshore) winds around 2100 PST (Figure 5). Dorman and Winant (2000) determined that winds in the western, central, and eastern Santa Barbara Channel exhibit different regimes, and the coastal station KSBA shares similarities with their termed "eastern regime," which is characterized by fairly weak and reversing winds compared to flow within the channel.

Similar to the coastal station, valley stations (KIZA and LPOC1) record maximum wind speeds from 1300 to 1500 PST (Figure 3) and exhibit dominant westerly wind direction between 1500 and 1700 PST (Figure 4). LPOC1 (located up valley; see Figure 1) is relatively far from the coast, and its location in a narrow portion of the SYV results in stronger mountain-valley and up-valley circulations (de Wekker et al., 1998; Rampanelli et al., 2004; Stull, 1988). The up-valley circulation appears as a relevant mechanism explaining the westerly wind direction at LPOC1 late afternoon and the relatively weaker average peak wind speed (~1 m/s). The most remarkable changes in wind direction at both valley stations are observed in late evening, contrasting with stations in the mountain and foothills where wind changes direction early in the evening. During the night, when a stratified stable boundary layer is well established near the surface, down-valley circulations driven by the rapid cooling of the mountain slopes and upper valley (Figure 1; de Wekker et al., 1998; Stull, 1988) may explain the eastward shift in wind direction observed at LPOC1 (Figure 5). Notice that the down-valley circulation seems to be less important at KIZA due to its geographic location in a wider part of the valley (Figure 1), corroborating with simulations in de Wekker et al. (1998).

3.3 | Extremes in winds using percentiles

This section investigates the statistics of extreme surface winds on a station-by-station basis using percentiles. Station analysis indicates that the strongest winds in coastal SB are recorded primarily at mountain stations in the early evening and from a northerly direction (Figures 3–5). When examining wind speed percentiles that consider all wind directions (Figure 6), the highest values are recorded at RHWC1, an expected result given that this station typically records the highest wind speeds seasonally and diurnally (Figures 2 and 3). Until approximately the 75th percentile, wind speed percentile values are below 5 m/s except for RHWC1. At the 75th percentile MPWC1 records the second-largest wind speed values (~5 m/s), followed by KIZA, KSBA, SBVC1, and MTIC1, respectively. The values at MTIC1 surpass all nonmountain stations at the 92nd percentile and surpass MPWC1 at the 97th percentile (Figure 6a). The rapid increase in values at MTIC1 indicates that this station typically records weak-to-moderate-strength winds (between 2 and 5 m/s) and occasionally records strong winds, exceeding 10 m/s with approximately 4% occurrence. The NWS-LOX Sundowner wind criteria (≥13.4 m/s) is reached at RHWC1 at the 95th percentile and at MTIC1 at the 99th percentile (Figure 6a). With the exceptions of MOIC1 and LPOC1, all other stations have reached these criteria for at least one observation (Figure 6b). Because gust data were not available at all stations, they were not included in this analysis.

3.4 | Sundowner wind criteria

When we consider hours with northerly (between 315° and 45°) winds exceeding 13.4 m/s (30 mph) or gusts exceeding 16.4 m/s (35 mph), all stations south of the SYM ridgeline have reached the NWS-LOX Sundowner wind criteria. Table 2 shows statistics for the percent of evening-to-morning hours (1800 to 0600 PST) that reached Sundowner wind criteria for the entire year and for each season individually. Focus in this section will be given for the entire year and for spring, which is the

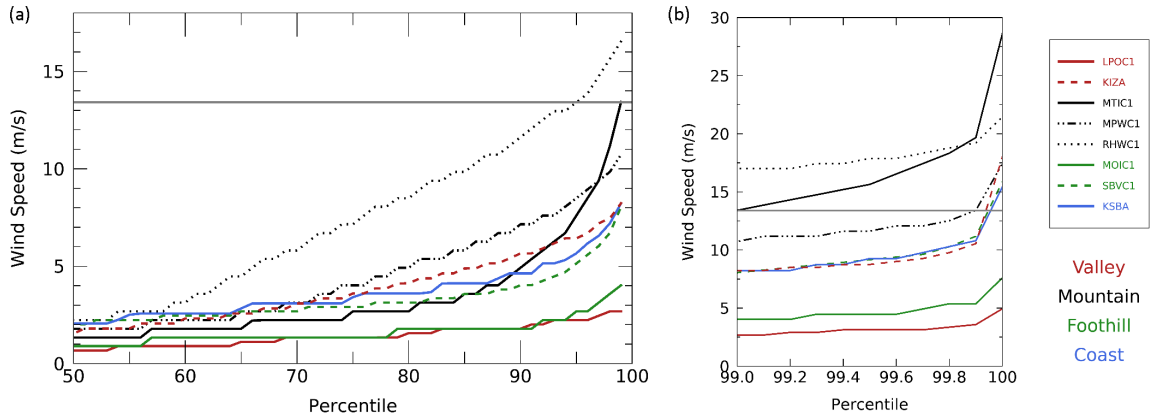

FIGURE 6 Wind speed percentiles by station from the (a) 50th to 99th percentiles and (b) 99th to 100th percentiles using data from the entire year. The maximum value is recorded as the value at the 100th percentile. The horizontal grey line indicates the NWS-LOX Sundowner criteria for sustained winds (13.41 m/s or 30 mph) [Colour figure can be viewed at wileyonlinelibrary.com]

TABLE 2 Statistics by-station on the total sample size (number of available hours for the entire time span), sundowner occurrences (the total number of hours reaching NWS-LOX Sundowner criteria), and the percentage of hours reaching Sundowner criteria

	MTIC1	MPWC1	RHWC1	MOIC1	SBVC1	KSBA
	All data					
Total sample size	85,994	17,263	17,264	39,194	38,602	97,377
Sundowner occurrences	4213	351	2705	45	344	25
% reaching Sundowner criteria	4.90	2.03	15.67	0.11	0.89	0.03
	By season					
	Winter (DJF)					
Total sample size	21,159	4603	4605	9338	9324	24,136
Sundowner occurrences	1126	55	440	17	108	10
% reaching Sundowner criteria	5.32	1.19	9.55	0.18	1.16	0.04
	Spring (MAM)					
Total sample size	21,614	4749	4747	9991	9531	24,718
Sundowner occurrences	1904	170	1104	22	152	9
% reaching Sundowner criteria	8.81	3.58	23.26	0.22	1.59	0.04
	Summer (JJA)					
Total sample size	21,556	4371	4373	10,423	10,306	24,408
Sundowner occurrences	266	92	748	2	31	1
% reaching Sundowner criteria	1.23	2.10	17.10	0.02	0.30	0.00
	Fall (SON)					
Total sample size	21,665	3540	3539	9442	9441	24,115
Sundowner occurrences	917	34	413	4	53	5
% reaching Sundowner criteria	4.23	0.96	11.67	0.04	0.56	0.02

Note: Recall that the NWS-LOX Sundowner criteria is northerly winds with either sustained speeds at least 13.4 m/s (30 mph) or gusts at least 15.6 m/s (35 mph). Statistics were calculated for the entire year (top three rows) and by season. Only the evening and early morning hours (1800 to 0600 PST) were considered in this analysis.

season with the peak of Sundowner events (Smith et al., 2018a; Jones et al., 2021) and the strongest winds (Figure 3). While there are no stations representative of conditions on the mountain ridge, simulations have shown that the strongest winds are observed in upper-to-mid slopes of the SYM in association with the lee-slope jet that characterizes Sundowner winds (Smith et al., 2018a; Duine et al., 2019, 2021; Carvalho et al., 2020; Jones et al., 2021). The mountain stations are placed where Sundowners are generally the strongest.

RHWC1 (west SYM) has the highest percentage of hours meeting Sundowner criteria, reaching 15.7% frequency considering overnight hours during all months and 23.3% frequency in overnight hours during only spring (Table 2). The station with the second-highest percentage of hours meeting the criteria is MTIC1 (east SYM) with 4.9% frequency in overnight hours considering all months and 8.8% frequency in overnight hours during spring. MPWC1 (central SYM) records frequencies of 2.0% and 3.6% for overnight hours considering all months and in spring only, respectively. All nonmountain stations record Sundowner wind criteria frequencies <1% for the entire year and <2% for spring only. SBVC1 on the foothills records the highest frequencies of nonmountain stations (0.9% considering all seasons and 1.6% in spring), whereas KSBA records the lowest (0.03% considering all seasons and 0.04% in spring; Table 2).

Next, we investigate the wind direction at each station when Sundowner wind criteria was met. Figure 7 displays the u (horizontal axis) and v (vertical axis) wind components in spring that reached Sundowner wind criteria, using both sustained wind and wind gust thresholds (reported at RAWS stations only; see Table 1 for the list of these stations). Sustained winds below 13.4 m/s are present when wind gusts exceeded 15.6 m/s at the time. To investigate systematic variations during the evening, the coloured dots indicate two 4-hr subsets: 1700-2000 PST and 2100-0000 PST. It is important to acknowledge that the station installation date (see Table 1) affects the data presented in Figure 7. RHWC1 and MTIC1 recorded the highest number of hours

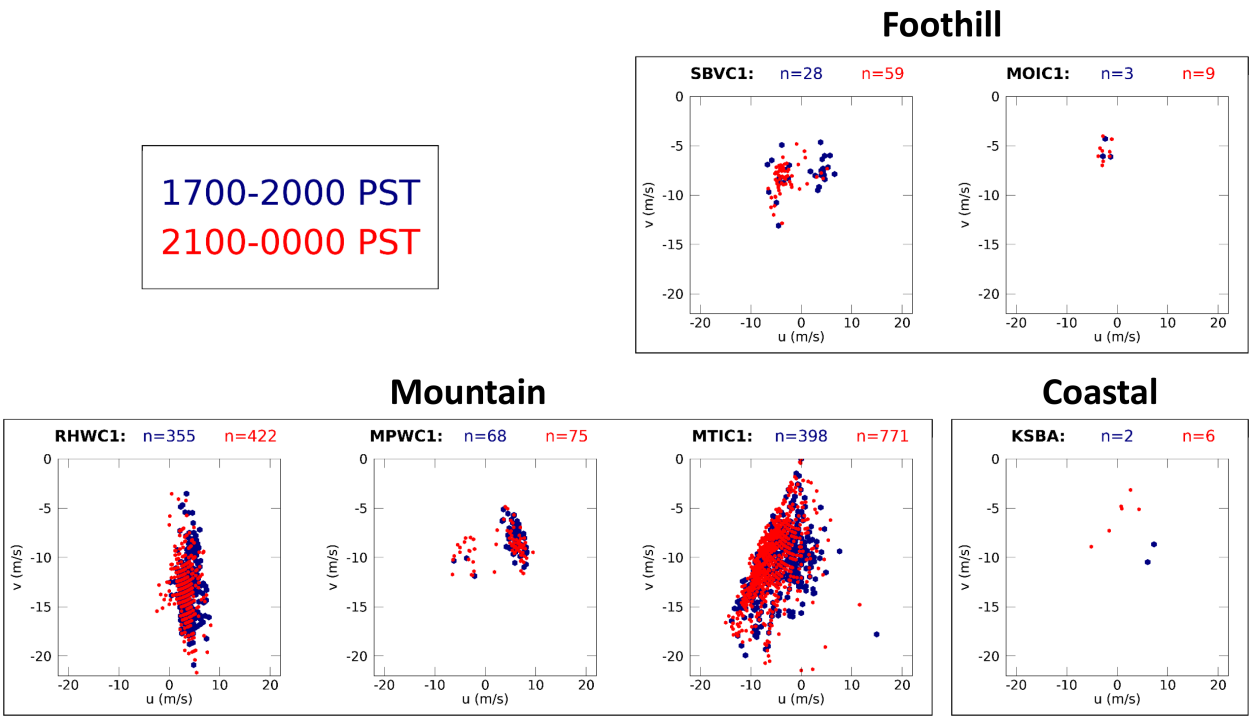

FIGURE 7 Scatterplots of u and v wind components (in m/s) during springtime hours reaching the NWS-LOX Sundowner criteria. Colours indicate time of day, broken into two 4-hr increments. Note that the period of installation differs among stations (see Table 1) and thus affects the potential number of hours that may reach Sundowner wind criteria [Colour figure can be viewed at wileyonlinelibrary.com]

reaching Sundowner wind criteria, even though there is a considerable difference in the total sample size of observations; RHWC was installed in July 2015, whereas MTIC1 was installed in January 2000 (Table 2). Contrastingly, KSBA recorded the fewest hours reaching these criteria despite having the longest observational record, indicating that only the strongest Sundowners, or Sundowners that occur with a retreated (further offshore) marine boundary layer, reach the coastal plain.

Wind direction during hours that reached Sundowner wind criteria is variable among mountain stations (Figure 7); RHWC1 records north-northwesterly winds, MPWC1 records northwesterly and northeasterly winds, and MTIC primarily records northeasterly winds. Foothill station MOIC1 records northeasterly winds and SBVC1 records both northeasterly and northwesterly winds. Therefore, patterns of wind direction during Sundowners are similar to those obtained in the climatology (Figures 4 and 5). These spatial differences in wind direction have been identified in the climatological simulations of Sundowners in Jones et al. (2021). The few hours during which Sundowner wind criteria was satisfied at KSBA (coastal) indicate predominantly northwesterly winds (Figure 7). Strong, offshore winds are rarely recorded at stations closer to the ocean. Duine et al. (2019) indicated that during Sundowners the wind speed maxima on mountain slopes quickly decreases in magnitude toward the coastal plain. Moreover, due to the proximity of the coast, cool and stably stratified marine air can be horizontally advected onto land during these events, preventing the lee jet from reaching ground level (Carvalho et al., 2020). Winds generally become more westerly in the later evening, from 2100 to 0000 PST compared to earlier where the easterly component is usually stronger (Figure 7). This pattern is most evident at RHWC1, MTIC1, and SBVC1.

3.5 | Correlations between buoy and land stations

The spatial and temporal variability in winds around Point Conception and in the Santa Barbara Channel are primarily controlled by a coastal jet. However, opposing winds associated with eddies may create a more complex three-layer system in some atmospheric conditions (Rahn et al., 2014). Typically, the SYM act as a barrier to the persistent northwesterly flow along the western California coastline, creating an expansion fan into the western SBC (Skyllingstad et al., 2001; Dorman and Koračin, 2008). In the presence of strong pressure gradients and a deep marine boundary layer, supercritical flow in the channel creates regions of wind acceleration and turning, or wind stress curl (Koracin et al., 2004). A

shallow MBL creates subcritical flow, and the jet accelerates around Point Conception quickly decelerates further into the channel.

Using an 11-year climatology from the WRF model at 2 km spatial resolution, Smith et al. (2018a, 2018b) postulated that Sundowners are in part caused by the inland propagation of the alongshore coastal California jet. That study indicated that the jet ranged between 600 and 1200 m above sea level in SYV during Sundowners, and was closer to the surface at locations further west. In the Sundowner regimes proposed in Jones et al. (2021), a strong coastal jet (>12 m/s) is present around Point Conception in the western regime, with northwesterly winds in the Santa Barbara Channel. However, during the eastern Sundowner regime, the coastal jet is weaker and does not extend into the Santa Barbara Channel.

To evaluate the relationship between observed winds during Sundowners and the coastal jet, we correlate winds at buoys and land stations. First, the seasonal and diurnal cycles of wind speed were calculated at the NDBC stations (Figure S3a). The strongest winds occur around and just south of Point Conception at PTGC1 (Point Arguello, CA) and b46054 (west SB channel) with means maximizing around 8.5 m/s in late spring and early summer, consistent with Dorman and Winant (2000). Maximum median wind speeds at b46011 (offshore to the west) and b46053 (east SB channel) are recorded in mid-spring around 6.5 and 5.5 m/s,

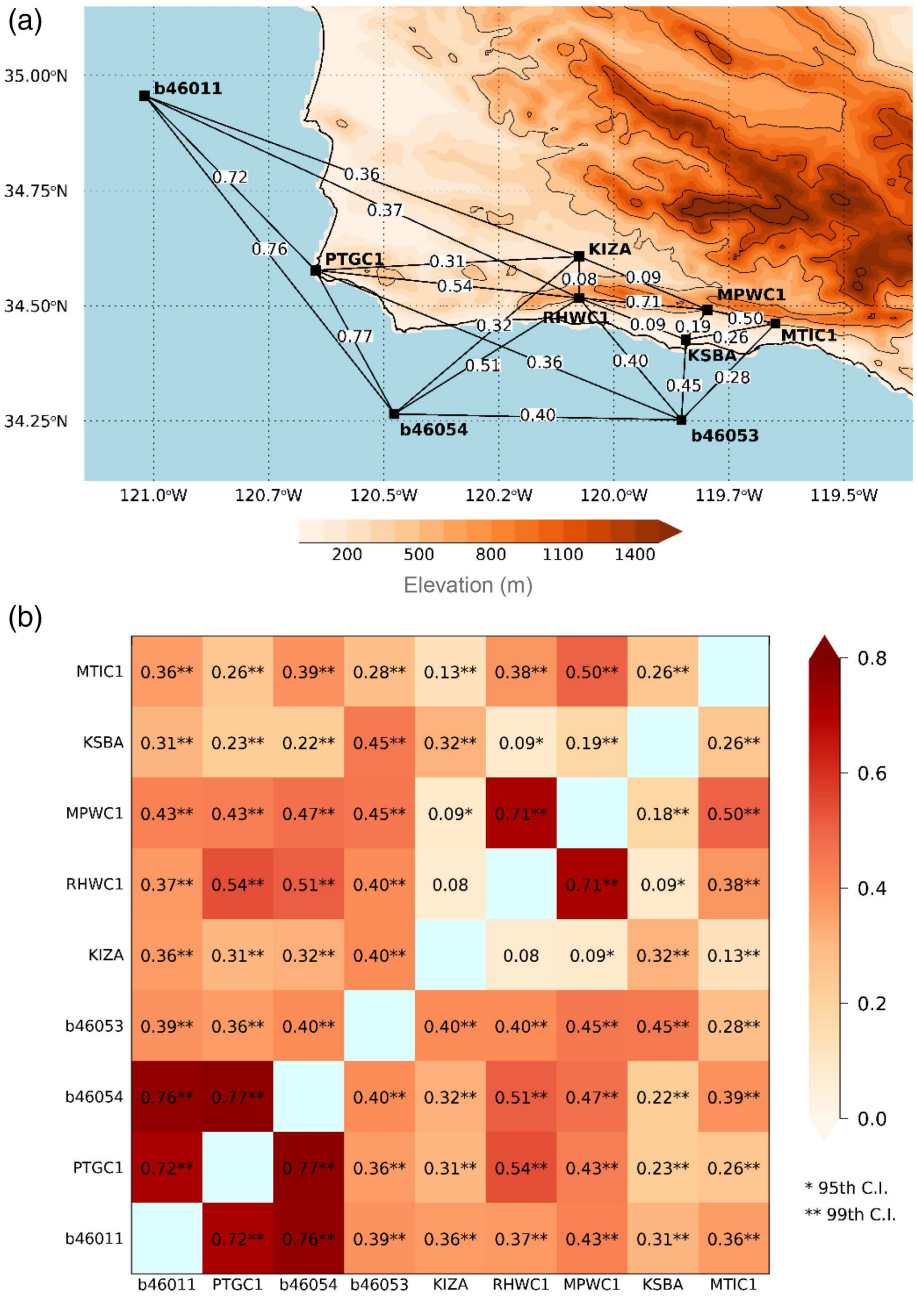

FIGURE 8 Correlations of wind speed in spring at 2000 PST. (a) Map of selected correlations between and among select land station and buoys. (b) Grid of all possible correlations, where values are repeated across the 1:1 axis. * indicates significance at the 95th confidence interval, and ** indicates significance at the 99th confidence interval [Colour figure can be viewed at wileyonlinelibrary.com]

respectively. The minimum mean wind speed at b46011 is 5 m/s in late summer, whereas at b46053, it reduces to 4 m/s in early winter.

Diurnally, maximum mean wind speeds at both PTGC1 (Point Arguello, CA) and b46054 (west SB channel) are around 8.5 m/s at 1900 PST, whereas b46053 (east SB channel) records maximum speeds (6 m/s) at 1700 PST, and b46011 (offshore, west) records maximum speeds (7 m/s) at 1600 PST (Figure S3b). Minimum values are recorded between 0800 and 1000 PST at all stations, with mean wind speeds ranging between 3.5 m/s at b46053 to 6.5 m/s at PTGC1 and b46054.

To examine relationships between the coastal jet and surface winds at land stations, we correlated winds at RHWC1 and MTIC1 with all four NDBC stations. Data was subset to include only spring (season with the highest frequency of Sundowners) at 2000 PST. This time was chosen since it marks the typical onset of strong winds on the slopes of the SYM during spring according to models and observations (Carvalho et al., 2020; Jones et al., 2021). Figure 8a shows linear correlations between NDBC stations and five land stations (RHWC1, MTIC1, MPWC1, KIZA, KSBA). Correlations between all of these stations are shown in Figure 8b. No lag was applied in these figures. All data that had matching times between stations was used, and results were maintained if only days or hours with Sundowners (i.e., NWS Sundowner criteria was met at RHWC1 or MTIC1) were investigated (not shown).

Correlations (*R*-values) calculated in this study are similar to the correlations of summer mean surface winds in Dorman and Winant (2000), which correlated wind speed along the wind direction principal axis in summer. Western buoys b46011, PTGC1, and b46054 are moderate-to-highly correlated among each other (0.72–0.77). The eastern buoy (b46053) is typically decoupled from other buoys, demonstrated through the lower correlations with western buoys (0.36–0.40). Instead, b46053 has slightly higher correlations with land stations KSBA and MPWC1 (0.45 for both), due to the various regimes that commonly dominate wind flow in the SB Channel (Dorman and Winant, 2000).

The coastal station (KSBA) has low correlations with all stations, ranging between 0.09 to 0.26 at other land stations analysed and 0.22 to 0.45 at buoy stations. In particular, the correlations are very low between KSBA and RHWC1 (0.09) and KSBA and MTIC1 (0.26), and the correlation between RHWC1 and MTIC1 is low-to-moderate (0.38). While relatively far in distance compared to distance between other stations, RHWC1 and MPWC1 record a moderate-to-high wind speed correlation (0.70), which is likely related to strong winds recorded from the north-northwesterly wind direction at both stations. The valley station KIZA has the lowest correlations with RHWC1 and MPWC1, which can be explained by the influence of the up-valley circulation discussed before, which contrasts with the mechanisms driving winds at higher elevations on the mountain slopes.

Lag correlations were calculated using buoy data in the 6 hr prior to 2000 PST to determine whether strong winds at a buoy preceded strong winds recorded at RHWC1 and MTIC1 (Figure S4). Correlations between buoys and the two land stations varied little with a lag applied (ranged <0.1). This indicates that there is no difference in phase observed at the surface between the peak of Sundowners and the intensification of winds in the Santa Barbara Channel or near Point Conception. Moreover, these findings show that there are moderate correlations between buoys and land stations RHWC1 (0.32–0.54) and MTIC1 (0.26–0.41), even when lags are applied (Figure S4). This process was repeated using the 6 hr prior to 1800 and 2200 PST, and similar results were found.

Despite the close proximity, circulation off the coast near Point Conception and in the SYV differs from circulation south of the SYM. This analysis indicated that strong near-surface winds on the SYM are positively correlated (at the 5% significance level) with each other and with buoy stations (Figure 8). In the western SYM, correlations between RHWC1 and buoys b46054 and PTGC1 are 0.51 and 0.54, respectively, while the correlation between RHWC1 and MPWC1 is 0.71 (which indicates a much stronger linear relationship). In the central and eastern SYM, the correlation between MPWC1 and MTIC1 is 0.50. However, in some cases, the correlation is very weak (i.e., 0.09 between KSBA and RHWC1). Similar correlation analysis was performed for conditions classified as "Sundowners" at RHWC1 (western SYM) and MTIC1 (eastern SYN) and results were very similar to those obtained for all days and conditions (not shown).

While this observational analysis cannot provide complete evidence of the relationship between the coastal jet and Sundowners, this study highlights that even though these correlations are positive, they are not strongly linear (r^2 <50%). This indicates the need for more observational and modelling studies investigating the complex interactions between the marine boundary layer, the coastal jet, the lee-slope jet, and local circulations to explain the spatial variability of winds in this region.

3.6 | Seasonal cycles, diurnal cycles, and Sundowner winds observed with the NOAA wind profiler

To understand local wind flow in the boundary layer, we investigated winds from the vertical wind profiler at the

Santa Barbara airport from the surface to 2600 m. Days with the strongest winds within the boundary layer (typically <1000 m AGL) and above are generally in winter and the weakest winds are in summer (Figure S5a). Patterns of wind direction vary diurnally and throughout the year at lower elevations, possibly linked to the diurnal circulations and the behaviour of the marine boundary layer as explained next.

Diurnally, close to the surface, wind speeds and wind directions are similar to the land-based KSBA station (Figure S5b). Nonetheless, the profiler shows some interesting aspects of the diurnal cycle within the boundary layer. For instance, on average, there is a transition between the nighttime easterlies and daytime westerlies in the mid-morning (between 0800 and 1,000 PST) within the lowest 600 m AGL. The transition is characterized by the weakest winds (<2 m/s). At 12 PST, winds strengthen and become southwesterly-to-westerly until 20 PST, when they transition back to easterlies. Above the boundary layer, winds rapidly accelerate. Another observation is that the mean wind direction at and above 1,200 m AGL is commonly from the northwest for most of the day, intensifying and turning into a northerly direction at approximately above 500 m AGL (possibly indicating the top of the boundary layer, consistent with modelling studies—e.g., Duine et al., 2019, 2021). This occurs around sunset, indicating the formation of a low-level (super-geostrophic) nocturnal jet that lasts only a few hours (Stull and Ahrens, 2000).

Of particular interest are the wind profiles on days with Sundowners. Figure 9 shows the profiler composite of wind speed and direction on days that did and did not record at least 1 hr reaching the NWS-LOX Sundowner criteria (see Section 3.4) between 18 and 06 PST at

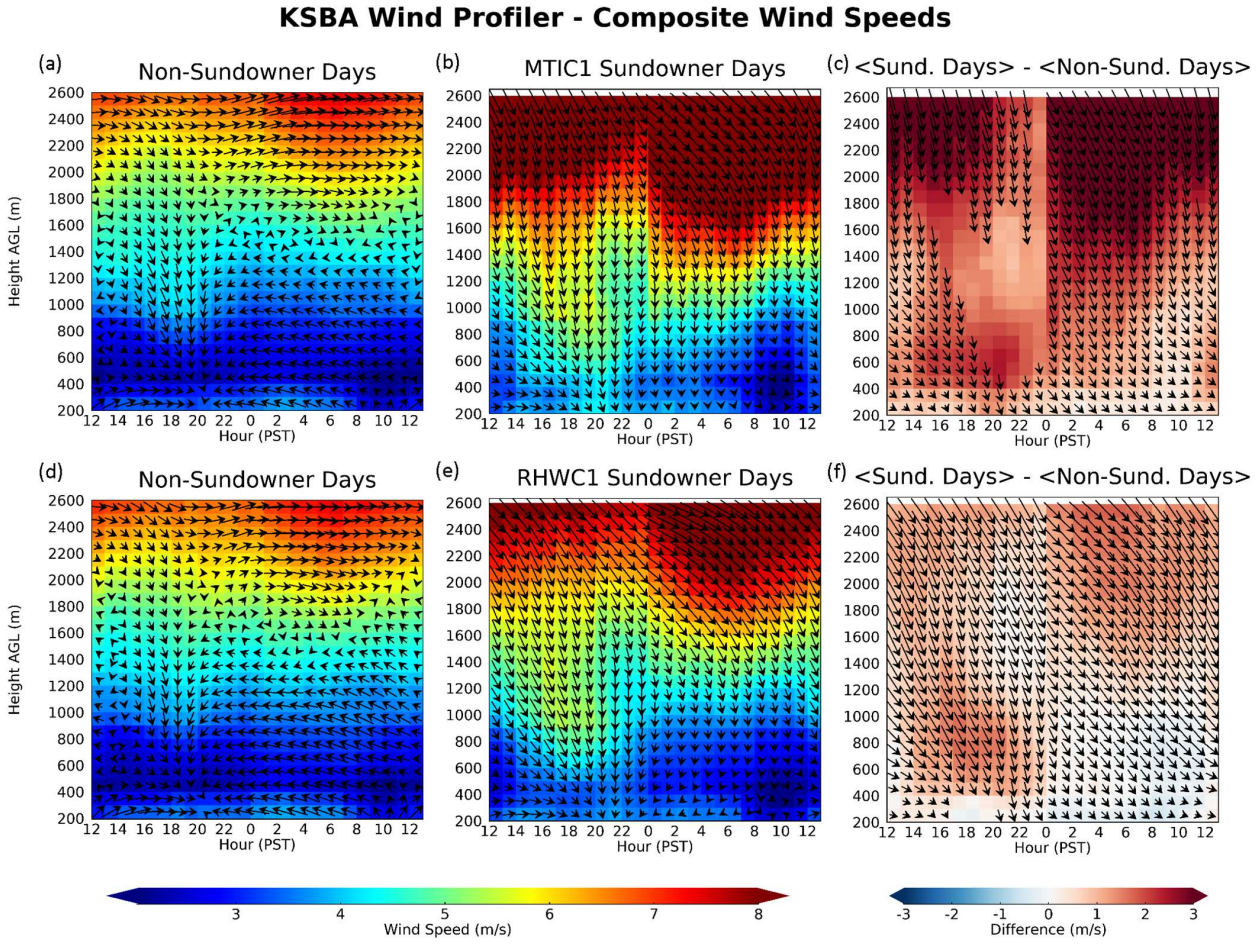

FIGURE 9 Wind speed and direction composites at the Santa Barbara airport vertical profiler for days when the NWX-LOX Sundowner criteria between 18 to 06 PST (a) were not reached for at least 1 hr at MTIC1 and (b) were reached for at least 1 hr at MTIC1. (c) Shows the difference between (a) and (b). Plots (d), (e), and (f) are the same as (a), (b), and (c) but at RHWC1. The u and v wind components were averaged to calculate composite wind directions in (a), (b), (d), and (e). The vectors were calculated for (c) and (f) by subtracting the u and v components for the Sundowner day composites (b, e) from the non-Sundowner composites (a, d). Only statistically significant vectors (determined by the Student's *t* test) are plotted [Colour figure can be viewed at wileyonlinelibrary.com]

MTIC1 (a–c) and RHWC1 (d–f). All seasons were used. In the difference plots (c, e), only vectors that are statistically significant at the 95th confidence interval are plotted.

During Sundowners recorded at MTIC1, wind speeds are up to 2 m/s stronger than non-Sundowner days from 14 to 22 PST typically between from 400 to 800 m AGL. The peak of these winds occurs around 20 PST, which is consistent with the observed characteristics of Sundowners. This peak in winds is linked to the intensification of winds associated with the lee-slope jet around sunset (Figure 9b). Notice that during this period, winds tend to change from NW during the day to NNW around sunset. Up to 200 m AGL, winds are weaker during the day, intensifying around 20 PST and weakening late in the evening. Nonetheless, strong northerly winds are observed above 1600 m AGL (Figures 9b,c), indicating the importance of synoptic forcing generating cross-mountain winds as a precursor of Sundowners (Cannon et al., 2017; Carvalho et al., 2020; Duine et al., 2021).

Relatively smaller differences are observed for wind profiler composites on Sundowner days at RHWC1 (Figure 9f); Wind speed between 500 and 1500 m is 1–2 m/s stronger than normal from 17 to 21 PST, and in the early morning hours, while below 400 m AGL there are less systematic changes in circulation. This is likely related to the fact that even during Sundowners, a strong stably stratified marine boundary layer may maintain the lee-slope jet above 200 m AGL as indicated in simulations in Carvalho et al. (2020) and Duine et al. (2021). In the upper levels, winds above 1,500 m are up to 2 m/s stronger with a stronger northwesterly component particularly from 02 to 12 PST. This may allude to the importance of upper-level dynamics producing Sundowners during the western regime (winds exhibit typically a NW direction), discussed in Jones et al. (2021) and Hatchett et al. (2018). Overall, analysis of data collected at the wind profiler demonstrates that both wind speed and direction differences are present when extreme, northerly winds are recorded at land-based stations. Mechanisms explaining the intensification of the jet have been investigated with radiosondes in Carvalho et al. (2020) and have been related to mountain wave activity and hydraulic jumps.

4 | VARIABILITY IN TEMPERATURE, RELATIVE HUMIDITY & DEW POINT DURING EXTREME WINDS

In Section 3, we highlighted the spatiotemporal variability of winds in coastal SB. Given the complex circulations in the SYV, SYM, and over the SB channel evident through the wind analysis, it is necessary to examine other meteorological variables such as temperature, relative humidity, and dew point to better understand atmospheric processes in this region. The seasonal and diurnal cycles for temperature, relative humidity, and dew point are shown in Figure S6. The seasonal and diurnal cycles for these variables will not be discussed. The reminder of this section is devoted to evaluating the behaviour of these variables during Sundowners.

4.1 | Temperature

While some studies have suggested that a temperature increase is one of the main characteristics during Sundowner events (Hatchett et al., 2018; Smith et al., 2018a), other studies have shown no evidence of a systematic signature in temperature ramps everywhere in the domain (Blier, 1998; Carvalho et al., 2020). Additionally, the spatiotemporal variability in temperature during Sundowners has not yet been examined based solely on observations. Figure 10 shows the diurnal median temperatures and the interquartile range (shaded) by season when NWS-LOX Sundowner criteria was not reached. Boxplots indicate the median, interquartile range, and minimum and maximum temperatures observed during hours reaching Sundowner criteria. All boxplots shown have medians that are statistically significantly different than temperature medians under non-Sundowner conditions. Hours without boxplots either had too few hours that reached Sundowner criteria (<10 instances) or the difference between median temperatures were not statistically significant.

At MTIC1 (east SYM), temperatures during strong winds vary depending on season and time of day (Figure 10, right column). In fall and winter, temperatures during strong, northerly (typically NE) winds are, on average, cooler than the seasonal median. It is possible that these dates are typically occurring in association with frontal systems. In contrast, temperatures during extreme winds in spring and summer are warmer than the seasonal normal, and the hours with statistically significant differences are in the evening and early morning. This warming is from mountain wave processes and adiabatic compression related to Sundowners (Blier, 1998; Cannon et al., 2017; Hatchett et al., 2018; Smith et al., 2018a; Carvalho et al., 2020).

At RHWC1, temperatures during extreme winds are frequently cooler than normal regardless of hour or season (Figure 10, left column), although the hours that have statistically significant differences in the median between temperatures during Sundowners and without Sundowners vary between seasons; the lower

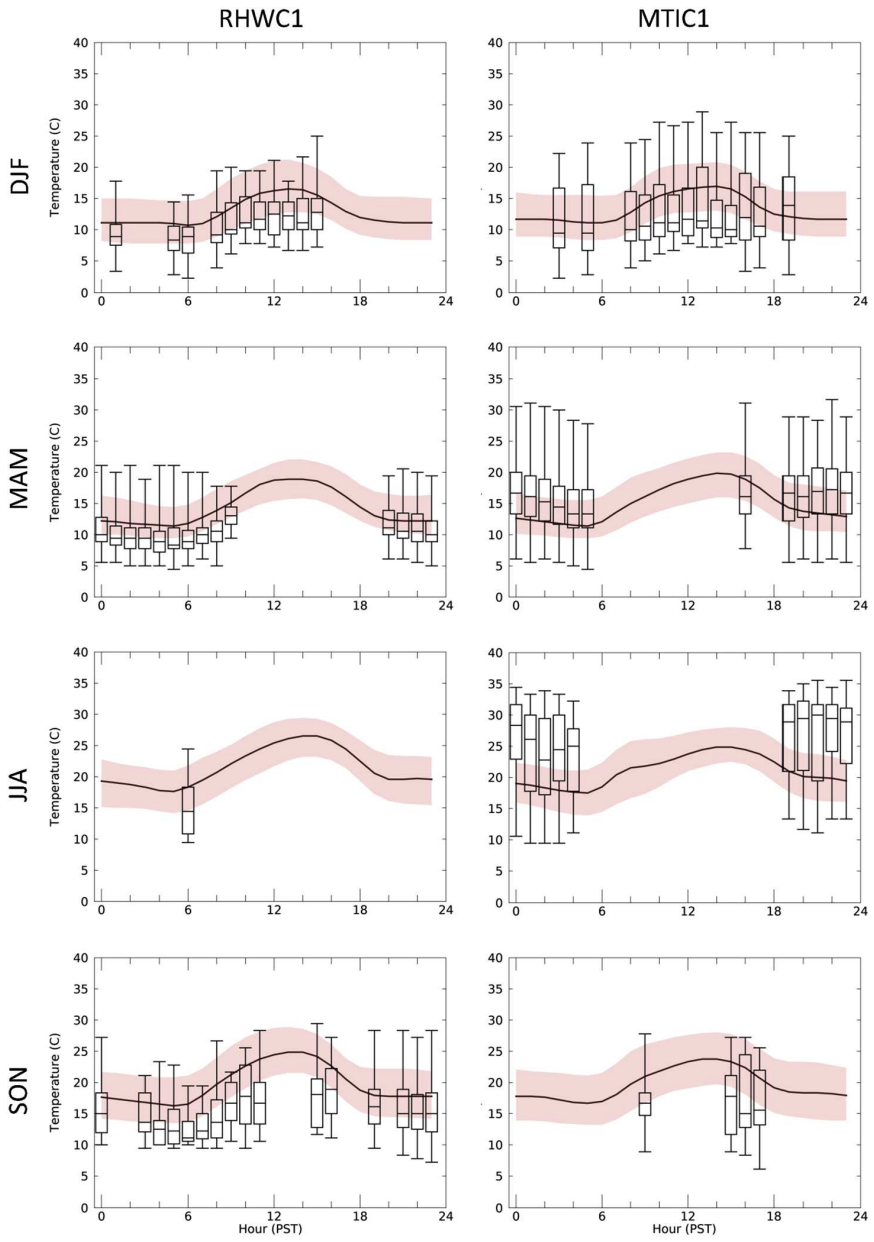

FIGURE 10 Diurnal cycles of median temperatures (thick black lines) and the interquartile range (red shading; 25th to 75th percentiles) of temperatures during non-Sundowner winds. Boxplots show the median, interquartile range, and minimum and maximum temperatures during Sundowner winds at MTIC1 (right) and RHWC1 (left) subset by season. The boxplots shown are statistically significant at the 95th confidence interval (when compared to the median temperature for that hour using all available data). See Section 2 for an explanation of the significance testing method [Colour figure can be viewed at wileyonlinelibrary.com]

temperatures during Sundowners in the morning and early afternoon are statistically significant in winter, whereas in spring the cooling is more evident in the evening and morning hours. This may also reflect the fewer cases during the other times. In summer, statistical significance is observed only at 06 PST, whereas lower temperatures seem to dominate throughout the day in fall. The lower temperatures during strong northerly winds at RHWC1 can be explained by the advection of cool oceanic air (from the Pacific Ocean) by the northwesterly winds, possibly in association with the intensification of the coastal jet, as exemplified in simulations of back-trajectories in Duine et al. (2021). Furthermore, this station is close to the ridgeline (Figures 1c and S1a,b) that partly diminishes the effect of adiabatic compression on temperatures (Carvalho et al., 2020).

4.2 | Dew point temperature (Td)

Similar to Figure 10, Figure 11 shows the diurnal median *Td* with the interquartile range during non-Sundowner conditions and boxplots for hours with statistically significant differences in the median *Td* during Sundowners. At MTIC1, the hours with statistically significant differences in the median vary between seasons, but commonly occur in the evening and/or morning. In spring, almost all hours (except 12 PST) have significant

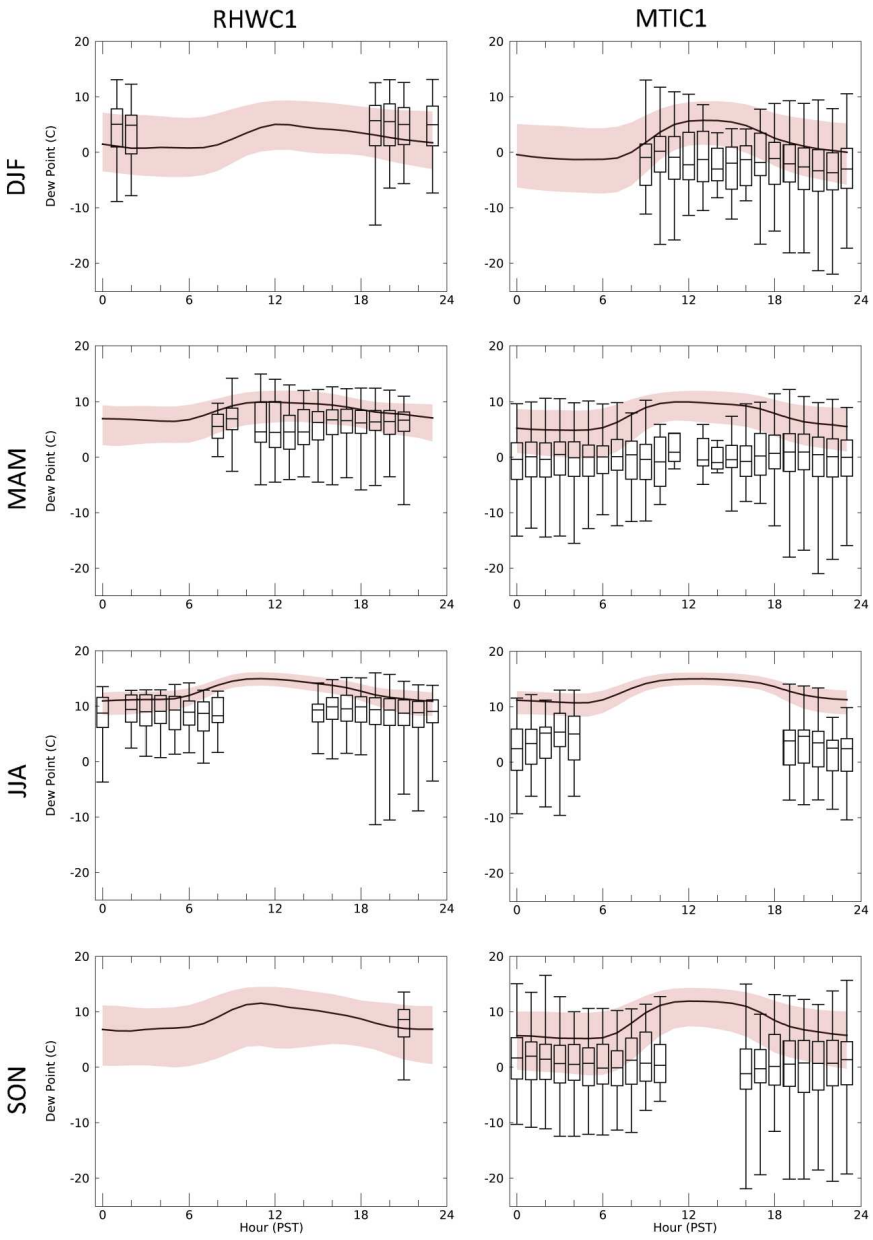

FIGURE 11 Similar to Figure 10 using dew point [Colour figure can be viewed at wileyonlinelibrary.com]

differences. During Sundowners, the median *Td* is typically lower than non-Sundowner conditions. This may be explained by the transport of dry air from levels above the mountain top to lower elevations, as indicated in the case study discussed in Carvalho et al. (2020) and shown through back trajectories in Duine et al. (2021). This is also suggested with results from the wind profiler (Figure 9).

At RHWC1, the median *Td* during Sundowners is higher than normal in the evening and early morning in fall and winter (Figure 11). This is possibly from the influence of moist oceanic air advected by the northwesterly winds as discussed before. In spring, the *Td* during strong northerly winds decrease relative to the non-Sundowner *Td* in the afternoon and evening. During summer, when the lower troposphere is warmer and drier, lower *Td* values are frequently observed in the evening and morning during strong Sundowners. It is important to note that fewer events have been observed at RHWC1 compared to MTIC1 due solely to differences in record length: approximately 4 years of data was examined at RHWC1 whereas nearly 20 years of data was examined at MTIC1 (Table 1).

The spatiotemporal variability of temperature and *Td* during strong, northerly winds illustrates the complexity of meteorological processes in this region. Nonetheless, the influence of strong cross-mountain (northerly) winds on *Td* (and thus, specific humidity) is quite evident and relevant, and may be a dominant factor in the low relative humidity often observed during these events.

Additional studies are necessary to determine the relative contributions of mountain waves in increasing adiabatic warming and subsequent drying, as well as horizontal advection. Evaluating patterns of temperature and *Td* during extreme cross-mountain winds has important implications in forecasting fire weather and improving wildfire preparedness.

5 | SPATIOTEMPORAL VARIABILITY OF THE FOSBERG FIRE WEATHER INDEX

Due to the large influence of wind speed on FFWI calculations, the seasonal cycle of the FFWI (Figure S6d) is unsurprisingly similar to wind speed (Figure 2), although the bimodal pattern is more pronounced with FFWI than wind speed. This is because maximum mean wind speeds are recorded in spring, but temperatures are higher in fall, increasing FFWI values for these two seasons. FFWI values peak at all stations except LPOC1 in spring, averaging between 16 to 20 at mountain stations and between 3 to 10 at nonmountain stations. Similar values are recorded in fall, separated by relative minima in summer at most stations. On a diurnal timescale, the FFWI cycle (Figure S6h) resembles the wind speed cycle (Figure 4); nonmountain stations record maximum FFWI values (between 5 and 24) in the early afternoon, whereas mountain stations record maximum values (between 12 and 26) in the evening. Seasonal variations in the diurnal cycles of FFWI were examined (not shown), and found that the timing of the minimum and maximum FFWI values is consistent in all seasons. The smallest (largest) values of FFWI were observed in winter (summer) due to a combination of colder (warmer) weather and wetter (drier) conditions.

To examine the frequency of significant fire weather (FFWI ≥50) at each station, we calculated percentiles of FFWI values (Figure 12). Overall, the strong winds at mountain stations result in the highest FFWI percentile values; RHWC1 reaches the significant FFWI threshold in all seasons, MTIC1 reaches the threshold in all seasons except for summer, and MPWC1 reaches the threshold in summer. In winter, a combination of relatively low temperatures, higher precipitation, and weaker winds result in lower percentiles at nearly all stations. In spring, strong winds at MTIC1 greatly increase FFWI, and values above the 95th percentile are higher at MTIC1 than RHWC1; these values exceed 50, which is considered critical fire weather. In summer, high temperatures and reduced precipitation create higher percentile values, especially at RHWC1 which reaches the significant FFWI

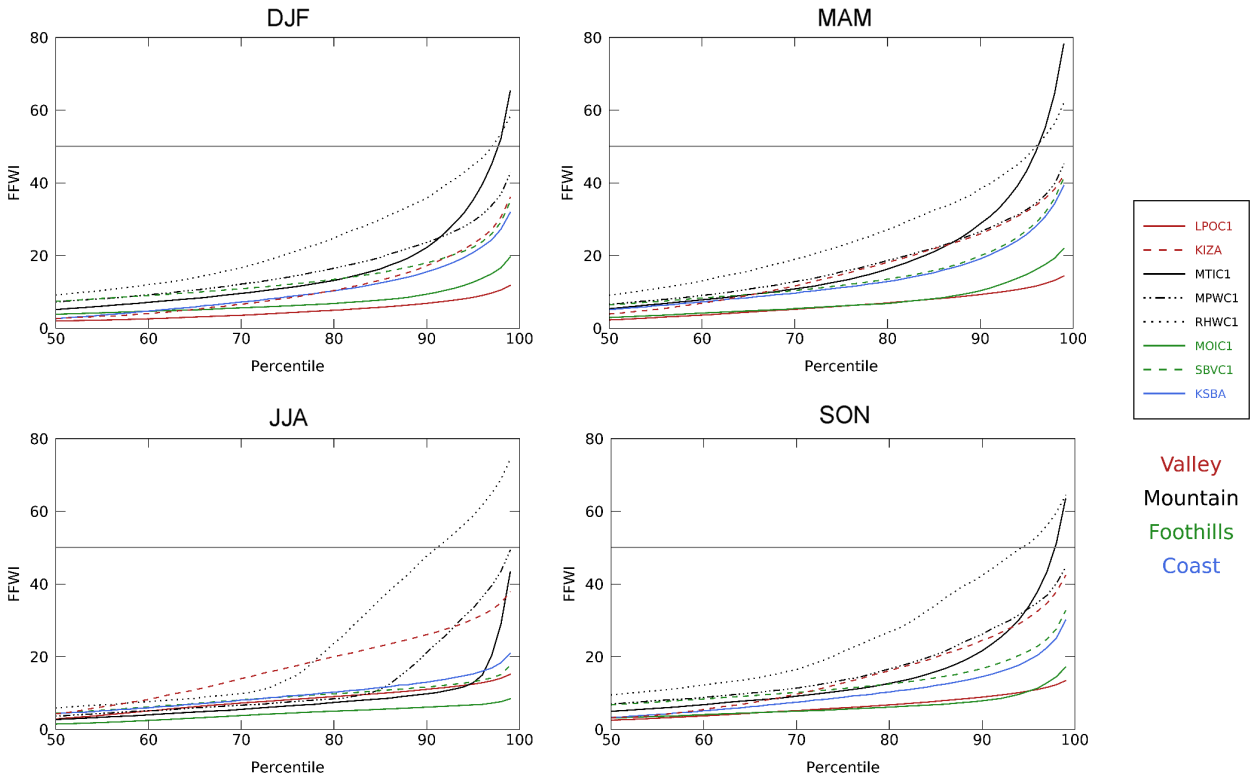

FIGURE 12 Percentiles of the FFWI for each season. The horizontal grey line indicates the threshold for significant fire weather conditions (FFWI ≥50) [Colour figure can be viewed at wileyonlinelibrary.com]

50 threshold at the 90th percentile. Additionally, KIZA records percentile values comparable with those found at mountain stations because of the similar wind speeds in summer (Figure 2). In fall, the percentiles are similar to winter due to decreasing temperatures and the beginning of the rainy season. It is important to note that all stations have recorded at least 1 hr with significant fire weather (see Figure S7).

6 | DISCUSSION AND CONCLUSIONS

Coastal Santa Barbara experiences extreme weather phenomena including strong, downslope wind events called Sundowners and significant fire weather conditions. This observational analysis characterized the spatiotemporal variability of winds in this region. Although the relatively low density of weather stations in coastal SB is not enough to fully explain Sundowner characteristics and mechanisms, an examination of data recorded at stations can complement previous studies that used high-resolution atmospheric models to examine winds, temperatures, and moisture in this region, and specifically Sundowner events. Our observational examination of yearly and diurnal cycles of wind indicates that, from a climatological perspective, the maximum speeds are observed in spring. Diurnally, the timing of maximum wind speed varies between mountain and nonmountain stations; winds at mountain stations peak in the evening (2000 to 2200 PST), whereas winds at nonmountain stations peak in the afternoon (1300 to 1400 PST). These results are consistent with previous model-based studies including Jones et al. (2021) and Hatchett et al. (2018).

Smith et al. (2018a) evaluated an 11-year climatology using WRF with 2 km grid cell resolution and created a "Sundowner Index" using the northerly wind component and temperatures differences between each grid cell and a peak (La Cumbre Peak) on the SYM ridgeline. Jones et al. (2021) examined 30 years of WRF at 1 km grid cell resolution and used combined empirical orthogonal function analysis to identify three Sundowner regimes: Eastern, Western, and Santa Barbara. In contrast, Smith et al. (2018a) argues that there is a continuum of Sundowners determined by wind direction at the SYM ridgeline rather than separate types. Furthermore, these simulations and observational analyses agree that a lee-slope jet forms on the southern SYM slopes during Sundowners, creating maximum wind speeds on the mountain slopes rather than near the ridgeline (Smith et al., 2018a; Carvalho et al., 2020; Duine et al., 2021; Jones et al., 2021).

Similarly, we found that mountain stations consistently record the strongest winds out of all stations, and the frequency of Sundowners (defined using the NWS-LOX criteria) varies greatly among stations (Table 2). This finding is consistent with Blier (1998) and Smith et al. (2018a) which state that stations far from the mountains such as KSBA do not record all Sundowner events due to the limited downstream extent of Sundowners and the influence of the marine boundary layer. During strong, cross-mountain (northerly) winds, variability in wind direction is evident; RHWC1 (west SYM) and MPWC1 (central SYM) record primarily northwesterly winds, and MTIC1 (east SYM) records northeasterly winds (Figures 5, 7, and 9). Using 4 years of hourly wind data from the NOAA wind profiler, we showed differences existing in winds within the marine boundary layer and aloft. The profiler characterized the nocturnal jet and showed differences in wind speed and direction when the NWS-LOX Sundowner criteria was reached at RHWC1 (western SYM) and MTIC1 (eastern SYM; Figure 9). These results reinforce the idea of eastern and western Sundowner regimes proposed in Jones et al. (2021). Moreover, weak-to-moderate wind speed correlations between RHWC1 and MTIC1 (0.38), and MPWC1 and MTIC1 (0.50; Figure 8), indicate linear relationships between strong winds on the eastern, central, and western SYM slopes are often not observed. The relationship between Sundowners and the coastal jet is noted in Smith et al. (2018a) and Jones et al. (2021) during the "western regime" only. In our study, correlations among and between land and buoy stations indicates that strong winds offshore are moderately correlated with western station RHWC1 and central station MPWC1, with correlations ranging between 0.37–0.54 and 0.43–0.47, respectively. However, there is no evidence of phase differences between the peaks of winds over land and in the Santa Barbara Channel based on lag-correlations between buoys and land stations MTIC1 and RHWC1, which may be expected in case of an eastward progression of winds as postulated in Smith et al. (2018a).

Temperature, *Td*, and the FFWI were additionally examined. During Sundowner winds, temperature variability may respond to a combination of effects, including temperature advection from upstream sources (Blier, 1998; Carvalho et al., 2020; Duine et al., 2021) and subsidence related to mountain wave development and the transport of air from above the mountain top (Blier, 1998; Carvalho et al., 2020; Jones et al., 2021). Additionally, warming was found in some, but not all, Sundowner case studies examined using observations and/or models (Ryan, 1996; Blier, 1998; Cannon et al., 2017; Hatchett et al., 2018; Carvalho et al., 2020).

During strong northerly winds in spring and summer, MTIC1 (west SYM) records temperature increases and dew point decreases in the evening and early morning hours (Figures 10 and 11), potentially from adiabatic warming and/or upstream influences (Duine et al., 2021). In contrast, RHWC1 records cooler temperatures and lower dew points during extreme winds, which may be from an oceanic influence. Similar to methods employed in Duine et al. (2021) and Carvalho et al. (2020), future study using back trajectory analysis could assist in determining the sources of air parcels, and may relate to or explain patterns observed in temperature and dew point during Sundowners.

Due to the large dependence on wind speed in the calculation, the seasonal and diurnal cycles of the FFWI are similar to wind speed; maximum values are typically recorded in spring and fall, and in the evening at mountain stations. Mountain stations record the highest frequency of critical fire weather conditions, although all stations have recorded significant fire weather. Some caveats are present when utilizing and interpreting this fire index. While temperatures are highest during summer and fuels are drier than winter and spring, relatively weaker winds decrease the FFWI values as a result of the large dependence on the index's reliance on wind speed. Additionally, it's important to note that the FFWI does not account for long-term trends in variables such as precipitation on seasonal and yearly scales (i.e., drought, excessive rainfall) and the respective role in fuel moisture, which are important factors concerning wildfire risk. Future study may be completed to create an operational product that incorporates the climatology of fire weather conditions with real-time data and fuel data to identify regions of high wildfire risk.

While the observational data investigated in this study have inherent caveats, including differences in station placement (i.e., ridge, valley) and different record lengths among stations, they provide valuable insight into actual surface conditions and allow for comparisons with Sundowner research that utilize atmospheric models. The addition of stations on the SYM ridgeline, in the Santa Ynez Valley, or in the San Rafael Mountains could benefit future studies, as collecting data from upstream sources may improve our understanding of conditions leading to Sundowners and extreme fire weather. Advancing knowledge on the variability and predictability of extreme winds and fire weather conditions with climatological studies can improve resource allocation (including the placement of new weather stations and other technical resources), and may contribute to wildfire mitigation, ultimately increasing resilience of the local community toward wildfires.

ACKNOWLEDGEMENTS

The authors acknowledge and appreciate collaborations with the National Weather Service—Los Angeles/Oxnard Office. We appreciate the suggestions made by the anonymous reviewers. This study was made possible by the agencies participating in the MesoWest data network (mesowest.utah.edu). Data for the wind profiler was provided by the NOAA/OAR/ESRL/PSL, Boulder Colorado, USA from their Web site at http://psl.noaa.gov/. This study was funded by the NSF-PREEVENTS ICER-1664173.

AUTHOR CONTRIBUTIONS

Katelyn Zigner: Conceptualization; data curation; formal analysis; investigation; methodology; project administration; resources; software; validation; visualization; writing-original draft; writing-review & editing. **Leila Maria de Carvalho:** Conceptualization; formal analysis; funding acquisition; investigation; methodology; project administration; resources; software; supervision; validation; writing-review & editing. **Charles Jones:** Conceptualization; formal analysis; funding acquisition; investigation; methodology; resources; software; supervision; validation; writing-review & editing. **Gert-Jan Duine:** Conceptualization; formal analysis; investigation; methodology; resources; software; validation; writing-review & editing.

ORCID

Katelyn Zigner https://orcid.org/0000-0002-3972-9195
Leila M. V. Carvalho https://orcid.org/0000-0002-8662-1953
Charles Jones https://orcid.org/0000-0003-4808-6977
Gert-Jan Duine https://orcid.org/0000-0002-9124-9252

REFERENCES

Bastin, S., Drobinski, P., Dabas, A., Delville, P., Reitebuch, O. and Werner, C. (2005) Impact of the Rhône and Durance valleys on sea-breeze circulation in the Marseille area. *Atmospheric Research*, 74, 303–328. https://doi.org/10.1016/j.atmosres.2004.04.014.

Blier, W. (1998) The sundowner winds of Santa Barbara, California. *Weather and Forecasting*, 13, 702–716. https://doi.org/10.1175/1520-0434(1998)013<0702:TSWOSB>2.0.CO;2.

Cannon, F., Carvalho, L., Jones, C., Hall, T., Gomberg, D., Dumas, J. and Jackson, M. (2017) WRF simulation of downslope wind events in coastal Santa Barbara County. *Atmospheric Research*, 191, 57–73. https://doi.org/10.1016/j.atmosres.2017.03.010.

Carvalho, L., Duine, G.J., Jones, C., Zigner, K., Clements, C., Kane, H., Gore, G., Bell, G., Gamelin, B., Gomberg, D., Hall, T., Johnson, M., Dumas, J., Boldt, E., Hazard, R. and Enos, W. (2020) The Sundowner winds experiment (SWEX) pilot study: understanding downslope windstorms in the Santa Ynez Mountains, Santa Barbara, CA. *Monthly Weather Review*, 148, 1519–1539. https://doi.org/10.1175/MWR-D-19-0207.1.

Countryman, C.M. (1972) *The Fire Environment Concept*. Berkeley, CA, USA: USDA Forest Service, p. 15.

de Wekker, S.F., Zhong, S., Fast, J.D. and Whiteman, C.D. (1998) A numerical study of the thermally driven plain-to-basin wind over idealized basin topographies. *Journal Applied Meteorology*, 37, 606–622. https://doi.org/10.1175/1520-0450(1998)037<0606:ANSOTT>2.0.CO;2.

Dorman, C.E. and Koračin, D. (2008) Response of the summer marine layer flow to an extreme California coastal bend. *Monthly Weather Review*, 136(8), 2894–2922. https://doi.org/10.1175/2007MWR2336.1.

Dorman, C.E. and Winant, C.D. (2000) The structure and variability of the marine atmosphere around the Santa Barbara Channel. *Monthly Weather Review*, 128, 261–282. https://doi.org/10.1175/1520-0493(2000)128<0261:TSAVOT>2.0.CO;2.

Duine, G.J., Hedde, T., Roubin, P., Durand, P., Lothon, M., Lohou, F., Augustin, P. and Fourmentin, M. (2017) Characterization of valley flows within two confluent valleys under stable conditions: observations from the KASCADE field experiment. *Quarterly Journal of the Royal Meteorological Society*, 143, 1886–1902. https://doi.org/10.1002/qj.3049.

Duine, G.J., Jones, C., Carvalho, L. and Fovell, R.G. (2019) Simulating sundowner winds in coastal Santa Barbara: model validation and sensitivity. *Atmosphere*, 10, 155. https://doi.org/10.3390/atmos10030155.

Duine, G.J., Carvalho, L.M.V., Jones, C. and Zigner, K. (2021) The effect of upstream topography on the onset of Sundowner winds in coastal Santa Barbara, CA. *JGR-Atmospheres*, 126(8), e2020JD033791. https://doi.org/10.1029/2020JD033791.

Ecklund, W.L., Carter, D.A. and Balsley, B.B. (1988) A UHF wind profiler for the boundary layer: brief description and initial results. *Journal of Atmospheric and Oceanic Technology*, 5(3), 432–441.

Fosberg, M.A. (1978) Weather in wildland fire management: the fire weather index. Proceedings of Conference on Sierra Nevada Meteorology, June 19-21, American Meteorological Society: Lake Tahoe, CA.

Giovannini, L., Laiti, L., Serafin, S. and Zardi, D. (2017) The thermally driven diurnal wind system of the Adige Valley in the Italian Alps. *Quarterly Journal of the Royal Meteorological Society*, 143, 2389–2402. https://doi.org/10.1002/qj.3092.

Goodrick, S.L. (2002) Modification of the Fosberg fire weather index to include drought. *International Journal of Wildland Fire*, 11, 205–211. https://doi.org/10.1071/WF02005.

Hatchett, B.J., Smith, C.M., Nauslar, N.J. and Kaplan, M.L. (2018) Brief communication: synoptic-scale differences between Sundowner and Santa Ana wind regimes in the Santa Ynez Mountains, California. *Natural Hazards and Earth System Sciences*, 18, 419–427. https://doi.org/10.5194/nhess-18-419-2018.

Hazra, A., Reich, B.J., Shaby, B.A. and Staicu, A.M. (2018) A semiparametric spatiotemporal Bayesian model for the bulk and extremes of the Fosberg fire weather index. *arXiv preprint*, 1812.11699.

Horel, J., Splitt, M., Dunn, L., Pechmann, J., White, B., Ciliberti, C., Lazarus, S., Slemmer, J., Zaff, D. and Burks, J. (2002) Mesowest: cooperative mesonets in the western United States. *Bulletin of the American Meteorological Society*, 83, 211–226. https://doi.org/10.1175/1520-0477(2002)083<0211:MCMITW>2.3.CO;2.

Jones, C., Fujioka, F. and Carvalho, L.M.V. (2010) Forecast skill of synoptic conditions associated with Santa Ana winds in Southern California. *Monthly Weather Review*, 138, 4528–4541.

Jones, C., Carvalho, L., Duine, G.J. and Zigner, K. (2021) A new climatology of Sundowner winds in coastal Santa Barbara, California, based on 30-yr high resolution WRF downscaling. *Atmospheric Research*, 138, 4528–4541. https://doi.org/10.1175/2010MWR3406.1.

Keeley, J.E., Safford, H., Fotheringham, C.J., Franklin, J. and Moritz, M. (2009) The 2007 southern California wildfires: lessons in complexity. *Journal of Forestry*, 106, 287–296.

Koracin, D., Dorman, C.E. and Dever, E.P. (2004) Coastal perturbations of marine-layer winds, wind stress, and wind stress curl along California and Baja California in June 1999. *Journal of Physical Oceanography*, 35, 1152–1173. https://doi.org/10.1175/1520-0485(2004)034<1152:CPOMWW>2.0.CO;2.

Li, D., Cova, T.J. and Dennison, P.E. (2019) Setting wildfire evacuation triggers by coupling fire and traffic simulation models: a spatiotemporal GIS approach. *Fire Technology*, 55(2), 617–642. https://doi.org/10.1007/s10694-018-0771-6.

Markowski, P. and Richardson, Y. (2010) *Mesoscale Meteorology in Midlatitudes*, Hoboken, NJ: Wiley.

McWethy, D.B., Schoennagel, T., Higuera, P.E., Krawchuk, M., Harvey, B.J., Metcalf, E.C., Schultz, C., Miller, C., Metcalf, A.L., Buma, B., Virapongse, A., Kulig, J.C., Stedman, R.C., Ratajczak, Z., Nelson, C.R. and Kolden, C. (2019) Rethinking resilience to wildfire. *Nature Sustainability*, 2(9), 797–804. https://doi.org/10.1038/s41893-019-0353-8.

Miller, R.K., Field, C.B. and Mach, K.J. (2020) Barriers and enablers for prescribed burns for wildfire management in California. *Nature Sustainability*, 3(2), 101–109. https://doi.org/10.1038/s41893-019-0451-7.

Moritz, M.A., Moody, T.J., Krawchuk, M.A., Hughes, M. and Hall, A. (2010) Spatial variation in extreme winds predicts large wildfire locations in chaparral ecosystems: extreme winds and large wildfires. *Geophysical Research Letters*, 37, L04801. https://doi.org/10.1029/2009GL041735.

Nadeau, D.F., Pardyjak, E.R., Higgins, C.W., Huwald, H. and Parlange, M.B. (2013) Flow during the evening transition over steep alpine slopes. *Quarterly Journal of the Royal Meteorological Society*, 139, 607–624. https://doi.org/10.1002/qj.1985.

National Weather Centre Los Angeles/Oxnard. (2021). 830 NWS LA, Oxnard.Retrieved from: https://www.wrh.noaa.gov/lox/fire_weather/redflag.pdf

National Wildfire Coordinating Group (2014) Interagency Wildland Fire Weather Station Standards & Guidelines. National Wildfire Coordinating Group: Boise, ID, USA, Vol. PMS 426-3, 55.

Parish, T.R., Rahn, D.A. and Leon, D. (2014) Aircraft observations of the marine boundary layer adjustment near point Arguello, California. *Journal of Applied Meteorology and Climatology*, 53 (4), 970–989. https://doi.org/10.1175/JAMC-D-13-0164.1.

Rahn, D.A., Parish, T.R. and Leon, D. (2014) Coastal jet adjustment near point conception, California, with opposing wind in the bight. *Monthly Weather Review*, 142, 1344–1360. https://doi.org/10.1175/MWR-D-13-00177.1.

Rampanelli, G., Zardi, D. and Rotunno, R. (2004) Mechanisms of up-valley winds. *Journal of the Atmospheric Sciences*, 61, 3097–3111. https://doi.org/10.1175/JAS-3354.1.

Rothermel, R.C. (1983) How to Predict the Spread and Intensity of Forest and Range Fires; Research Paper INT-GTR-143; U.S. Department of Agriculture, Forest Service, Intermountain Forest and Range Experiment Station: Ogden UT, USA. Doi: https://doi.org/10.2737/int-gtr-143.

Ryan, G. (1991) *Sundowner Winds*. Weather Service Office: Santa Maria, CA, USA, p. 18.

Ryan, G. (1996) Downslope winds of Santa Barbara, California. National Oceanic and Atmospheric Administration Technical Memorandum NWS WR-240, Scientific Services Division, Western Region, Salt Lake City, Utah, USA.

Skyllingstad, E.D., Barbour, P. and Dorman, C.E. (2001) The dynamics of northwest summer winds over the Santa Barbara Channel. *Monthly Weather Review*, 129(5), 1042–1061. https://doi.org/10.1175/1520-0493(2001)129<1042:TDONSW>2.0.CO;2.

Smith, C., Hatchett, B. and Kaplan, M. (2018b) Characteristics of Sundowner winds near Santa Barbara, CA, from a dynamically downscaled climatology: environment and effects aloft and offshore. *Journal of Geophysical Research: Atmospheres*, 123(23), 13092–13110.

Smith, C.M., Hatchett, B.J. and Kaplan, M.L. (2018a) Characteristics of sundowner winds near Santa Barbara, California, from a dynamically downscaled climatology: environment and effects near the surface. *Journal of Applied Meteorology and Climatology*, 57, 589–606. https://doi.org/10.1175/JAMC-D-17-0162.1.

Stull, R.B. (1988) *An Introduction to Boundary Layer Meteorology*. Springer Science & Business Media. Hingham, MA: Kluwer Academic Publishers.

Stull, R.B. and Ahrens, C.D. (2000) *Meteorology for Scientists and Engineers*. 2, Florence, KY: Brooks/Cole.

Sukup, S. (2013) Extreme northeasterly wind events in the hills above Montecito, California. Western Region Technical Attachment NWS WR-1302. National Weather Service Western Region, Salt Lake City, UT.

Thompson, M.P., Bowden, P., Brough, A., Scott, J.H., Gilbertson-Day, J., Taylor, A., Anderson, J. and Haas, J.R. (2016) Application of wildfire risk assessment results to wildfire response planning in the southern Sierra Nevada, California, USA. *Forests*, 7(3), 64. https://doi.org/10.3390/f7030064.

Zigner, K., Carvalho, L., Peterson, S., Fujioka, F., Duine, G.J., Jones, C., Roberts, D. and Moritz, M. (2020) Evaluating the ability of FARSITE to simulate wildfires influenced by extreme, downslope winds in Santa Barbara, California. *Fire*, 3, 29. https://doi.org/10.3390/fire3030029.

SUPPORTING INFORMATION

Additional supporting information may be found online in the Supporting Information section at the end of this article.

How to cite this article: Zigner, K., Carvalho, L. M. V., Jones, C., & Duine, G.-J. (2022). Extreme winds and fire weather in coastal Santa Barbara County, CA: An observational analysis. *International Journal of Climatology*, *42*(1), 597–618. https://doi.org/10.1002/joc.7262